



American Society of Hematology
 2021 L Street NW, Suite 900,
 Washington, DC 20036
 Phone: 202-776-0544 | Fax 202-776-0545
 editorial@hematology.org

The proto-oncogene *TCL1A* deregulates cell cycle and genomic stability in CLL

Tracking no: BLD-2022-015494R1

Johanna Stachelscheid (University Hospital Cologne, Germany) Qu Jiang (University Hospital Cologne, Germany) Christoph Aszyk (University Hospital of Cologne, Germany) Kathrin Warner (University Hospital Cologne, Germany) Nadine Bley (Martin Luther University Halle-Wittenberg, Germany) Tony Müller (University of Cologne (UoC), Germany) Olga Vydzhak (University Hospital Cologne, Germany) Konstantinos Symeonidis (University Hospital Cologne, Germany) Giuliano Crispazza (University Hospital Cologne, Med1, Germany) Petra Mayer (University Hospital Cologne, Germany) Stuart Blakemore (University of Cologne, Germany) Gudrun Goehring (Department of Human Genetics, Hannover Medical School, Hannover, Germany, Germany) Sebastian Newrzela (Goethe-University Clinic, Germany) Stephanie Hippler (University Hospital Cologne, Germany) Sandra Robrecht (University Hospital of Cologne, Germany) Karl-Anton Kreuzer (University at Cologne, Germany) Christian Pallasch (University hospital of Cologne, Germany) Marcus Krüger (University Cologne, Germany, Germany) Axel Lechner (University of Göttingen, Germany) Kirsten Fischer (University Hospital Cologne, Germany) Stephan Stilgenbauer (Saarland University Medical Center, Germany) Dirk Beutner (University Medical Center Göttingen, Germany) Michael Hallek (University of Cologne, Germany) Daniel Auguin (University of d'Orléans, INRA, USC1328, France) Stefan Hüttelmaier (Martin Luther University Halle-Wittenberg, Germany) Johannes Bloehdorn (Internal Medicine III, University Hospital Ulm, Germany) Elena Vasyutina (University of Cologne, Germany) Marco Herling (University Hospital Cologne, Department I of Internal Medicine, Germany)

Abstract:

Upregulation of the proto-oncogene *TCL1A* is causally implicated in various B-cell and T-cell malignancies. High-level *TCL1A* correlates with aggressive disease features and inferior clinical outcomes. However, the molecular and cell-biological consequences of, particularly nuclear, *TCL1A* are not fully elucidated. We observed here in mouse models of subcellular-site specific *TCL1A*-induced lymphomagenesis, that *TCL1A* exerts a strong transforming impact via nuclear topography. In proteomic screens of *TCL1A*-bound molecules in CLL cells and B-cell-lymphoma lines, we identified regulators of cell cycle and DNA repair pathways as novel *TCL1A* interactors, particularly enriched under induced DNA damage and mitosis. Via functional mapping and *in-silico* modeling, we specifically identified the mitotic checkpoint protein *CDC20* as a direct *TCL1A* interactor. According to a regulatory impact of *TCL1A* on the activity of the *CDC20*-containing mitotic checkpoint and anaphase-promoting complexes during mitotic progression, *TCL1A* overexpression accelerated cell-cycle transition in B-cell-lymphoma lines, impaired apoptotic damage responses in association with pronounced chromosome mis-segregation, and caused cellular aneuploidy in *Eμ-TCL1A* mice. Among hematopoietic cancers, *CDC20* levels seem particularly low in CLL. *CDC20* expression negatively correlated with *TCL1A* and lower expression marked more aggressive and genetically unstable disease and cellular phenotypes. Knock-down of *Cdc20* in *TCL1A*-initiated murine CLL promoted aneuploidy and leukemic acceleration. Taken together, we discovered a novel cell-cycle associated effect of *TCL1A* abrogating controlled cell cycle transition. This adds to our concept of oncogenic *TCL1A* by targeting genome stability. Overall, we propose that *TCL1A* acts as a pleiotropic adapter molecule with a synergistic net effect of multiple hijacked pathways.

Conflict of interest: No COI declared

COI notes:

Preprint server: No;

Author contributions and disclosures: E. Vasyutina, J. Stachelscheid, Q. Jiang, C. Aszyk, M. Hallek, S. Stilgenbauer, J. Bloehdorn, and M. Herling designed the experiments and analyzed the in-vitro generated data. E. Vasyutina, J. Stachelscheid, C. Aszyk, Q. Jiang, T. Müller, O. Vydzhak, K. Symeonidis, and P. Mayer performed the in-vitro experiments. E. Vasyutina, K. Warner, G. Crispatzu, and S. Newrzela designed, performed, and analyzed the in vivo experiments and GEP data of mice. MS experiments and statistical analyses were performed by M. Krueger, J. Stachelscheid and C. Aszyk. G. Goehring, S. Hippler, and K.A. Kreuzer performed cytogenetic analyses. A. Lechner and D. Beutner acquired human tissue samples. N. Bley and S. Hüttelmaier performed PLA experiments. J. Bloehdorn, S. Robrecht, K. Fischer, and S. Stilgenbauer acquired and analyzed GEP and clinical data of the CLL8 trial, S.J. Blakemore and C. Pallasch performed scRNA-seq data analysis, D. Auguin performed the molecular modelling and the in-silico analysis of protein complexes. E. Vasyutina, J. Stachelscheid, and M. Herling wrote the manuscript.

Non-author contributions and disclosures: No;

Agreement to Share Publication-Related Data and Data Sharing Statement: For original data, please contact the corresponding author. Microarray data are available at GEO under accession number GSE126595 (CLL8, doi:10.1038/s41467-021-25403-y) and GSE192409 (murine GEP data, access token yxixgmcclbsrfwt). The MS-based proteomics data are deposited at the ProteomeXchange Consortium via the PRIDE partner repository with the dataset identifiers PXD029961 (Reviewer account details: Username: reviewer_pxd029961@ebi.ac.uk, password: vwUPNzn7), PXD030776 (Username: reviewer_pxd030776@ebi.ac.uk, password: WcTGtb2y), and PXD030773 (Username: reviewer_pxd030773@ebi.ac.uk, password: b2Cx0OLM). Analyzed MS data and GEP data from mice are given in the Supplements.

Clinical trial registration information (if any):

1 The proto-oncogene TCL1A deregulates cell cycle and ge- 2 nomic stability in CLL

3 Johanna Stachelscheid¹⁻³, Qu Jiang¹⁻³, Christoph Aszyk¹⁻³, Kathrin Warner^{1,4}, Nadine
 4 Bley⁵, Tony Müller¹⁻³, Olga Vydzhak¹⁻³, Konstantinos Symeonidis¹⁻³, Giuliano Cris-
 5 patzu¹⁻³, Petra Mayer¹⁻³, Stuart James Blakemore¹⁻³, Gudrun Goehring⁶, Sebastian
 6 Newrzela⁴, Stephanie Hippler¹, Sandra Robrecht¹, Karl-Anton Kreuzer¹, Christian
 7 Pallasch¹⁻³, Marcus Krueger^{2,3}, Axel Lechner⁷, Kirsten Fischer¹, Stephan Stilgenbau-
 8 er^{8,9}, Dirk Beutner⁷, Michael Hallek¹⁻³, Daniel Auguin¹⁰, Stefan Hüttelmaier⁵, Johan-
 9 nes Bloehdorn^{8,#}, Elena Vasyutina^{1-3,t,#}, and Marco Herling^{1-3,11,#}

¹⁰ Department I of Internal Medicine, Center for Integrated Oncology Aachen-Bonn-
¹¹ Cologne-Duesseldorf (CIO ABCD), University Hospital Cologne, Cologne, Germany;

¹²Center for Molecular Medicine Cologne (CMMC), University of Cologne, Cologne,
¹³Germany; ³Cologne Excellence Cluster on Stress Responses in Aging-Associated

¹⁴ Diseases (CECAD), University of Cologne, Cologne, Germany; ⁴Senckenberg Institute
¹⁵ of Pathology, Goethe-University, Frankfurt/M., Germany; ⁵Institute of Molecular

¹⁶ Medicine, Section for Molecular Cell Biology, Faculty of Medicine, Martin Luther University
¹⁷ Halle-Wittenberg, Charles Tanford Protein Center, Halle, Germany; ⁶Institute

¹⁸ of Human Genetics, Hannover Medical School, Hannover, Germany; ⁷Department of
¹⁹ Otorhinolaryngology, University of Göttingen, Göttingen, Germany; ⁸Department of

²⁰ Internal Medicine III, Ulm University, Ulm, Germany; ⁹Department of Internal Medi-
²¹ cine I, Saarland University Medical Center, Homburg, Germany; ¹⁰University of d'Or-

lénas, INRA, USC1328, 45067 Orléans, France and Structural Motility, Institut Curie, CNRS, UMR 144 Paris, France; and ¹¹Department of Hematology, Cellular Therapy,

24 and Hemostaseology, University of Leipzig, Leipzig, Germany
25

26

[#] Authors contributed equally

[†] Deceased February 24, 2020

29

Corresponding author:

30 Marco Herling, MD

31 Tel. +49 341 9713846, Fax: +49 221 47898339

82 Email: marco.herling@medizin.uni-leipzig.de

B3

84 Running title: Cell cycle ablation and genome instability by TCL1

Keywords: TCL1A / lymphocytic leukemia / mitotic checkpoint / CDC20 / aneuploidy

86

37 Abstract: 248 words

38 Main text: 4397 words

Figure count: 7 main Figures and 10 Supplemental Figures

10 Table count: 0 main
11 Refs: 1-56

43 **Key points**

- 44 • TCL1A directly engages CDC20 in the mitotic checkpoint complex, accelerating
45 cell cycle transit and driving genome instability in B-cells
46 • Downregulated CDC20 in CLL cells resembles the aneuploidy phenotype and is
47 associated with more aggressive disease and cellular features

48 **Abstract**

49 Upregulation of the proto-oncogene TCL1A is causally implicated in various B-cell
50 and T-cell malignancies. High-level TCL1A correlates with aggressive disease fea-
51 tures and inferior clinical outcomes. However, the molecular and cell-biological con-
52 sequences of, particularly nuclear, TCL1A are not fully elucidated. We observed here
53 in mouse models of subcellular-site specific TCL1A-induced lymphomagenesis, that
54 TCL1A exerts a strong transforming impact via nuclear topography. In proteomic
55 screens of TCL1A-bound molecules in CLL cells and B-cell-lymphoma lines, we iden-
56 tified regulators of cell cycle and DNA repair pathways as novel TCL1A interactors,
57 particularly enriched under induced DNA damage and mitosis. Via functional map-
58 ping and *in-silico* modeling, we specifically identified the mitotic checkpoint protein
59 CDC20 as a direct TCL1A interactor. According to a regulatory impact of TCL1A on
60 the activity of the CDC20-containing mitotic checkpoint and anaphase-promoting
61 complexes during mitotic progression, TCL1A overexpression accelerated cell-cycle
62 transition in B-cell-lymphoma lines, impaired apoptotic damage responses in asso-
63 ciation with pronounced chromosome mis-segregation, and caused cellular aneu-
64 ploidy in *Eμ-TCL1A* mice. Among hematopoietic cancers, *CDC20* levels seem partic-
65 ularly low in CLL. *CDC20* expression negatively correlated with *TCL1A* and lower
66 expression marked more aggressive and genomically unstable disease and cellular
67 phenotypes. Knock-down of *Cdc20* in TCL1A-initiated murine CLL promoted aneu-
68 ploidy and leukemic acceleration. Taken together, we discovered a novel cell-cycle
69 associated effect of TCL1A abrogating controlled cell cycle transition. This adds to
70 our concept of oncogenic TCL1A by targeting genome stability. Overall, we propose
71 that TCL1A acts as a pleiotropic adapter molecule with a synergistic net effect of
72 multiple hijacked pathways.

73 **Introduction**

74 T-cell leukemia/lymphoma 1A (*TCL1A*) is the prototypic member of a 3-paralogue
75 family that further includes *TCL1B* and Mature T-cell proliferation 1 (*MTCP1*). Upreg-
76 ulation of *TCL1A* due to rearrangements of its gene locus at chromosome 14 is con-
77 sidered the initiating event in T-prolymphocytic leukemia (T-PLL).^{1,2} Deregulated
78 *TCL1A* is also implicated in the pathogenesis of chronic lymphocytic leukemia
79 (CLL).³

80 Both T-PLL and CLL show elevated *TCL1A* expression in >90% of cases, yet at vari-
81 able levels. Highest levels are associated with more complex karyotypes, high-risk
82 (cyto)genetic aberrations, unfavorable clinical features, such as faster tumor cell
83 doubling^{2,4–6}, and poorer responses to chemo-immunotherapies.^{4–7} Analogous obser-
84 vations were made in other B-cell lymphomas.^{8–10}

85 The transforming capacity of *TCL1A* in T- and B-cells has been demonstrated in
86 transgenic (tg) mouse models. Animals expressing human *TCL1A* under the murine
87 T-cell specific *Lck* promoter or the B-cell receptor (BCR) *VH*-promoter/*IGHμ*-
88 enhancer develop expansions that closely resemble human T-PLL (*Lck*^{pr}-*TCL1A*
89 mice)¹¹ or CLL (*Eμ-TCL1A* mice)¹², respectively.

90 The 14kDa β-barrel-shaped *TCL1A* protein lacks enzymatic properties and does not
91 possess DNA-binding activity. Its best-established oncogenic function is an adapter-
92 like engagement of induced homo-dimers in sub-plasmalemmal molecular complex-
93 es with AKT, leading to nuclear translocalization and catalytic augmentation of this
94 oncogenic serine/threonine kinase.^{13,14} *TCL1A* can also enhance NF-κB and inhibit
95 AP-1 transcriptional activities.¹⁵ We characterized *TCL1A* as a threshold-lowering
96 ‘sensitizer’ toward antigen receptor signals, mainly mediated by an activating physi-
97 cal interaction with involved cytoplasmic kinases.^{5,6,16} As constitutively active
98 myristoylated (myr) AKT in murine B-cells does not recapitulate the oncogenic effect
99 of *TCL1A*¹⁷, we postulate an under-recognized target pleiotropism of *TCL1A*.¹⁸ Par-
100 ticularly, the molecular effectors of nuclear *TCL1A* are not well established.

101 We also observed a cell-cycle dependent protein expression of *TCL1A* at the single-
102 cell level in CLL and other B-cell tumors.^{4,9} This implicates *TCL1A* as an intricate
103 component of deregulated cell cycle pathways, which are central to B-cell leukemo-
104 genesis.^{19–21}

105 Generally, the checkpoints that regulate cell cycle progression after DNA replication
106 are the G2/M checkpoint, which ensures DNA integrity before prophase entry, and
107 the mitotic checkpoint (also known as spindle assembly checkpoint), which prevents

108 premature cell division until all kinetochores are attached to a spindle.^{22,23} The mitotic
109 checkpoint is maintained by the mitotic checkpoint complex (MCC), which antagonizes
110 the multi-subunit anaphase-promoting complex (APC/C), an E3 ubiquitin-ligase
111 mediating onset of the anaphase. The cell division cycle 20 (CDC20) plays a crucial
112 role in both complexes. By acting as a coactivator of the APC/C (APC/C^{CDC20}), it
113 promotes anaphase initiation.²³ As part of the MCC, however, it also inhibits the func-
114 tion of APC/C^{CDC20} together with mitotic arrest deficient 2 (MAD2) and the mitotic
115 checkpoint proteins BUBR1 and BUB3.²⁴

116 Here, we demonstrate that TCL1A perturbs cell cycle transition and impedes an ade-
117 quate DNA damage response, resulting in genome instability. We implicate protein
118 interactions of TCL1A with components of the MCC and APC/C, such as CDC20, to
119 mediate these effects. Associations with aggressive disease characteristics and clin-
120 ical outcomes emphasize a central role of (deregulated) CDC20 in CLL.

121 **Materials and Methods**

122 **Patient material**

123 Peripheral-blood (PB) derived healthy-donor (Institutional Blood Bank) and CLL
124 samples (Departmental Biorepository) were obtained under IRB-approved protocols
125 (#11-319, #01-143, #9-1085, #13-091) with written informed consent according to the
126 Declaration of Helsinki. Ficoll-isolated PB mononuclear cells (PBMC) and B-cells
127 were purified and cultured as reported.²⁵

128 **Mouse experiments**

129 Studies on *Eμ-TCL1A* mice¹² were carried out under permission 84-02.04.2012.A394
130 (regional council Cologne, Germany). Preleukemic stage: white blood cell (WBC)
131 counts <25x10⁶/ml (age 7-8 weeks), no hepatosplenomegaly; overt leukemic stage:
132 >30% CD5⁺/19⁺ population in PB and a WBC >50x10⁶/ml.

133 For primary murine hematopoietic stem cell and progenitor cell (HSC/HPC) trans-
134 plantations (F21/03; FK/1050, regional council Darmstadt, Germany), bone marrow
135 (BM) cells were isolated from B6-SJL mice and lineage-committed cells depleted as
136 described.²⁶ Remaining cells were retrovirally transduced with vectors MP91-EGFP,
137 human(h)TCL1A, myr-hTCL1A, or -nuclear localization signal (nls)-hTCL1A. After
138 irradiation, 1x10⁶ transduced cells were transplanted into C57BL/6 recipients.

139 **Immunoprecipitations, mass spectrometry, and validations**

140 Immunoprecipitations (IPs) with specific antibodies were carried out using the follow-
141 ing beads: streptavidin-coupled (biotinylated proteins; Sigma, St. Louis, USA), anti-
142 FLAG M2 magnetic beads (FLAG-tagged proteins; Sigma), Ni²⁺ resins (his-tagged
143 proteins; Sigma), and Protein G Sepharose (Sigma) or Protein G magnetic Dyna-
144 beads (Invitrogen, Waltham, USA). Eluates and input samples were analyzed by
145 immunoblots. Samples and mass spectrometry (MS) protocols as well as details on
146 the proximity ligation assay and the protein complementation assay are provided in
147 the **Supplements**.

148 **Cell cycle analysis**

149 Cells were synchronized via nocodazole (Sigma) at 100ng/ml for 16h or with RO-
150 3306 (Selleckchem, Houston, USA) at 9μM for 20h. Cells were washed, released into
151 full medium, and harvested at indicated time points. Cellular DNA content was
152 measured by Hoechst 33258 (Sigma) staining in the presence of RNase A (Invitro-
153 gen) using the IntraPrep Permeabilization kit (Beckman Coulter, Brea, USA). Analy-
154 sis on the Gallios flow cytometer used the KALUZA software (both Beckman Coul-
155 ter).

156 **Profiling experiments**

157 Array-based gene expression profiles (GEP) were performed on tumor cell suspen-
158 sions (>70% B-cell content) from spleens of recipients of HSC/HPC transduced with
159 site-targeted TCL1A versions or with EGFP (CD19+GFP+ cells at day 100). Gene
160 set enrichment analysis (GSEA) used the GSEA_4.0.3 software (Broad Institute,
161 Cambridge, USA). Microarray GEP of 337 human CLL8 trial samples and data anal-
162 yses are outlined in **Supplements** and in ²⁷⁻²⁹. For single-cell RNA-sequencing of
163 splenocytes of *Eμ-TCL1A* mice see ³⁰ and **Supplements**.

164 **Data sharing**

165 For original data contact the corresponding author. Microarray data are available at
166 GEO under accession # GSE126595 (CLL8)²⁹ and GSE192409 (murine GEP data,
167 access token yxixgmclbsrfwt). The MS-based proteomics data are deposited at the
168 ProteomeXchange Consortium via the PRIDE³¹ partner repository with the dataset
169 identifiers PXD029961 (Reviewer account details: Username:
170 reviewer_pxd029961@ebi.ac.uk, password: vwUPNzn7), PXD030776 (Username:
171 reviewer_pxd030776@ebi.ac.uk, password: WcTGtb2y), and PXD030773
172 (Username: reviewer_pxd030773@ebi.ac.uk, password: b2Cx0OLM).

173 **Results**

174 **TCL1A exerts a strong oncogenic impact via its nuclear localization**

175 TCL1A is expressed in the cytoplasm and in the nucleus of CLL cells (**Supplemental**
176 **Figure 1A**). To refine a concept of subcellular-site specific leukemogenic effects of
177 TCL1A, we transduced murine HSC/HPC with three human *TCL1A* variants: wild
178 type (*wt*), membrane-targeted myr-TCL1A, and nuclear-localized nls-TCL1A (**Figure**
179 **1A**). Localization of these TCL1A forms was validated in HEK293T cells and *in situ*
180 (spleens of induced lymphomas) (**Figure 1B, Supplemental Figure 1B**). Mice trans-
181 planted with cells expressing nls-hTCL1A had a significantly shorter lymphoma-
182 specific survival in comparison to mice with *wt*-TCL1A induced tumors (median 349
183 days vs 388 days, respectively; **Figure 1C**), despite similar disease characteristics
184 and histologies (**Supplemental Figure 1C**). All three groups developed mostly B-cell
185 leukemias/lymphomas and less frequently CD4/CD8 double-positive/negative T-cell
186 leukemias/lymphomas (**Supplemental Table 1**). GSEA of GEP data from the B-cell
187 tumors identified nuclear pathways including DNA repair, cell cycle, and mitotic spin-
188 dle to be enriched in the nls-hTCL1A vs *wt*-TCL1A induced lymphomas (**Figure 1D-**
189 **E, Supplemental Table 2**). These pathways were also enriched in all TCL1A condi-
190 tions compared to GFP control B-cells (**Supplemental Figure 2**). We concluded a
191 preferential B-cell oncogenic function of TCL1A in the nuclear compartment, espe-
192 cially in the context of DNA repair and cell cycle regulation.

193 **TCL1A is part of protein complexes that regulate DNA damage response and**
194 **cell cycle**

195 To characterize TCL1A's interactome in a more unbiased fashion, MS analyses of
196 TCL1A-IPs were performed in human CLL samples (N=11, **Supplemental Table 3**;
197 divided into U-CLL (IGHV unmutated) and M-CLL (**Figure 2A**) or into three cytoge-
198 netic/clinical-risk categories (**Supplemental Figure 3**) and in tonsillar B-cells (N=3).
199 In total, 889 and 459 TCL1A-interacting proteins were identified in tonsillar B-cells
200 and CLL cells, respectively (groups vs IgG-control; FCh>2, FDR q-value<0.05, **Sup-**
201 **plemental Table 4**). The interactome of TCL1A was independent of disease subset,
202 as most interacting partners overlapped across the genetic and clinical categories
203 (**Figure 2B, Supplemental Figure 3B**). Over-representation analysis (ORA) identi-
204 fied a variety of pathways within the TCL1A interactome in CLL, suggesting a plei-
205 otropic perturbation of cellular processes by TCL1A. Among them, several nuclear
206 pathways were identified, including 'cell cycle' as the third largest functional network
207 cluster identified in the TCL1A interactome, further emphasizing the relevance of
208 nuclear TCL1A (**Figure 2C-D, Supplemental Figure 4, Supplemental Table 5**). It

209 included important proteins regulating cell cycle transition, such as the protein kinase
210 ATM (G2/M checkpoint, DNA repair)³², MCM proteins (DNA replication checkpoint)³³,
211 and NEK9 (mitotic checkpoint)³⁴ (**Figure 2E-F**). These findings suggest an important
212 role of TCL1A in the regulation of the DNA-damage response (DDR) and cell cycle
213 transition.

214 **TCL1A interacts with proteins of the mitotic checkpoint complex**

215 This novel pronunciation of nuclear effectors of TCL1A prompted us to analyze the
216 interactome of TCL1A after specific activation signals, i.e. genotoxic stress and mito-
217 sis induction, in the B-PLL-derived cell line JVM3 (hardly expresses TCL1A). Stable
218 overexpression of TCL1A (JVM3^{TCL1A}) conferred a phenotype of resistance to the
219 classical DNA-targeting chemotherapeutics doxorubicin, cyclophosphamide, and
220 etoposide (**Supplemental Figure 5**). MS analysis of TCL1A-pulldowns from
221 JVM3^{TCL1A} vs JVM3^{GFP} cells, that were a) left untreated, b) exposed to DNA-damage
222 induction (etoposide), or c) synchronized in enforced mitosis (nocodazole), identified
223 a total of 962 TCL1A-interacting proteins (FCh>2, FDR q-value<0.05; **Figure 3A-B**,
224 **Supplemental Tables 6-7**), with a marked increase after genotoxic or mitotic stimu-
225 lation (total of 76 in condition a) vs 245 in b) vs 736 in c); **Figure 3B**). Most TCL1A-
226 interacting proteins were exclusively detected in mitosis (N=674), whereas 164 pro-
227 teins specifically bound to TCL1A under genotoxic stress.

228 The functional pathway clusters within these TCL1A interactomes identified by ORA
229 were highly dependent on the condition (**Figure 3C-D, Supplemental Tables 8-10**).
230 Under genotoxic stress and mitosis, ‘cell cycle’ and ‘cell cycle checkpoints’ were
231 highly prominent recurrent pathways, with ‘cell cycle’ being the second biggest clus-
232 ter in the TCL1A interactome of JVM3 cells synchronized in mitosis (**Figure 3C**). Im-
233 portantly, proteins involved in the regulation of the APC/C, as components of the
234 MCC (e.g. CDC20, MAD2) or subunits of the APC/C (e.g. CDC27), were specifically
235 present in the mitosis condition, suggesting a function of TCL1A in the composition
236 and regulation of the mitotic checkpoint (**Figure 3E**). We confirmed the interaction of
237 TCL1A with CDC20, MAD2, and CDK1 in B-cells of *Eμ-TCL1A-tg* mice and in human
238 CLL cells via co-IP (**Figure 4A-B**).

239 **TCL1A accelerates cell cycle transition of mitotic B-cells**

240 Investigating the impact of TCL1A on mitotic progression, we observed that the
241 TCL1A-positive variants of JVM3, DoHH2, MEC1, and HEK293T cells had transi-
242 tioned faster through mitosis already three to five hours after release from G2 syn-
243 chronization, as compared to TCL1A-negative controls (**Figure 4C-E; Supplemental**
244 **Figure 6A**). Protein levels of the APC/C targets cyclin A and CDC20 degraded faster

245 in TCL1A-positive cells. Furthermore, phosphorylation of central regulators of the
246 G2/M-checkpoint, including CDK1, that decline along the course of mitosis^{22,35},
247 showed lower levels after release in TCL1A-positive cells (**Figure 4E, Supplemental**
248 **Figure 6B**). Phosphorylation of Aurora A/B/C, all involved in the mitotic checkpoint,
249 was not markedly altered by TCL1A overexpression (**Supplemental Figure 6C,D**).

250 To specifically dissect the effect of TCL1A on mitotic transit, we performed *in-vivo*
251 BrdU S-phase labeling experiments in leukemic *Eμ-TCL1A* vs *wt* mice. Splenocytes
252 were isolated 20h after BrdU injection and stained for incorporated BrdU and phos-
253 phorylated Histone3 (p-H3) as a marker for active mitosis. *Eμ-TCL1A* splenocytes
254 showed significantly increased proliferation over *wt* splenocytes, indicated by a high-
255 er number of BrdU+ ($P=0.009$) and p-H3+ ($P=0.012$) cells. A larger proportion of *Eμ-*
256 *TCL1A* cells had exited mitosis within 20h after injection (BrdU+/p-H3- cells, $P=0.01$).
257 There were also significantly more BrdU-/pH3+ cells ($P=0.01$) in the *Eμ-TCL1A* group
258 after the BrdU pulse (**Figure 4F**). According to these data, TCL1A-positive B-cells
259 enter and exit the cell cycle more frequently, implicating abnormal cell cycle passag-
260 ing.

261 **Aberrant DNA-damage response and aneuploidy in TCL1A-driven leukemia**

262 We next investigated the impact of aberrant TCL1A expression on central regulators
263 of the DDR, i.e. ATM and p53. In primary CLL cells, high TCL1A levels (by qRT-
264 PCR) correlated with reduced levels of phospho-activated and cleaved ATM upon
265 genotoxic stress (**Figure 5A,B**). Furthermore, B-cells from *Eμ-TCL1A* mice show
266 reduced p53 levels accompanied by an accumulation of TUNEL-positive double-
267 strand breaks as compared to B-cells from age-matched *wt* mice (**Figure 5C**).

268 Considering the observed protein interactions of TCL1A with MCC components, we
269 investigated whether TCL1A negatively affects mitotic spindle formation and segre-
270 gation, leading to increased chromosomal aberrations. Indeed, TCL1A-positive JVM3
271 and DoHH2 cells showed a higher frequency of multipolar spindles than their TCL1A-
272 negative controls ($P=0.032$, $P=0.029$, respectively), which was corroborated by
273 shRNA-mediated TCL1A knock-down in MEC1 cells ($P=0.041$) (**Figure 5D**). Addi-
274 tionally, we identified a higher number of polyploid cells in the DoHH2^{TCL1A} and
275 JVM3^{TCL1A} lines compared to empty-vector controls ($P=0.006$ and $P=0.005$, respec-
276 tively; **Figure 5E**) alongside a trend to more complex karyotypes (**Figure 5F**).

277 In line with these findings, chromosomal aberrations were frequently detected in B-
278 cells from *Eμ-TCL1A* mice (**Figure 5G**), with aneuploidy already present at the pre-
279 leukemic phase ($P=0.03$) and even more pronounced at the overt leukemic stage
280 ($P<0.0001$; **Figure 5H**). These data implicate overexpressed TCL1A to perturb ge-

281 nomic integrity via impaired DNA damage responses and aberrant spindle formation
282 (chromatid segregation).

283 **TCL1A and CDC20 directly interact during mitosis**

284 To assess the involvement of TCL1A in the MCC, we investigated the interaction of
285 TCL1A with selected targets. Proximity ligation assays (PLAs) identified interactions
286 of TCL1A with CDC20, MAD2, and the G2/M checkpoint protein CDK1 in the cyto-
287 plasm as well as along the spindles of MEC1 cells (**Figure 6A, Supplemental Fig-**
288 **ure 7A,B**). The TCL1A-CDC20 interaction increased from interphase to prophase
289 and persisted during mitosis (**Figure 6B, Supplemental Figure 7C,D**).

290 As CDC20 is one of the key proteins controlling mitotic checkpoint transition, we vali-
291 dated the interaction of TCL1A with CDC20 by split-reporter protein complementation
292 assay (PCAs)³⁶, which facilitate intracellular detection of direct protein-protein inter-
293 actions based on complementation of N/C-terminal YFP components (**Figure 6C**).
294 Immunofluorescence microscopy of HeLa cells harboring TCL1A-YFP^N and CDC20-
295 YFP^C constructs demonstrated a direct TCL1A-CDC20 interaction, which accumulat-
296 ed at the mitotic plate and dispersed during anaphase (**Figure 6D**). Homodimeriza-
297 tion of TCL1A was not a prerequisite for this interaction, as *wt* TCL1A and the dimer-
298 ization-defective mutant PLT^{3A} equally bound to CDC20 (**Supplemental Figure 7E**).

299 **Defined sites in CDC20 are involved in the interaction with TCL1A**

300 CDC20 activity is controlled by several regulatory sequences such as the KEN- and
301 CRY-boxes, which are targets of phosphorylation and which engage APC/C sub-
302 strates.^{23,37,38} The C-boxes facilitate interaction with the APC/C³⁸, whereas the
303 MAD2-interacting motif (MIM) is required for the interaction with MAD2. To identify
304 functional motifs of CDC20 involved in the interaction with TCL1A, we generated five
305 CDC20 mutants: (i) del97-169 lacking KEN-, MIM-, and CRY-box; (ii) RCRY^{4A}:
306 R132>A and CRY165-167>AAA (inactivating MIM- and CRY-box); (iii) R^A: R132>A
307 (inactivating MIM-box); (iv) CRY^{3A}: CRY165-167>AAA (inactivating CRY-box); (v)
308 KEN^{3A}: KEN97-99>AAA (inactivating KEN-box) (**Figure 6E**). The mutations in the
309 KEN, CRY, and MIM motifs are described not to alter the protein structure of
310 CDC20.³⁹

311 Expression vectors encoding TCL1A were co-transfected into HEK293 cells along-
312 side one of the CDC20 mutants or CDC20^{wt} constructs. Subsequent co-IPs revealed
313 that mutations in the KEN sequence (KEN^{3A}) did not affect the CDC20-TCL1A inter-
314 action. Mutations in the CRY-box (CRY^{3A}) led to a slightly reduced CDC20-TCL1A
315 interaction. Interestingly, aa substitutions in the MIM sequence (R132A; R^A), resulted

316 in a significantly impaired CDC20-TCL1A interaction. A simultaneous mutation of
 317 MIM and CRY sequences (RCRY^{4A}) or a deletion of the KEN, MIM, and CRY se-
 318 quences (del97-169) almost completely abolished the interaction (**Figure 6E**).

319 ***In-silico* modeling resolves the CDC20-TCL1A complex structure**

320 To refine and validate our model derived from this functional motif mapping, we per-
 321 formed a thorough *in-silico* prediction of the CDC20-TCL1A complex based on pub-
 322 lished experimental protein structures of CDC20 (pdb ID 4GGA) and TCL1A (pdb ID
 323 1JSG) using CPoRT and HADDOCK 2.2.^{40,41} CDC20 contains a central core of a 7-
 324 bladed β-propeller and two mobile extensions at the N- and C-termini.⁴² Importantly,
 325 the 4 aa that were involved in the interaction with TCL1A (C165, R166, Y167, R132)
 326 are located at the N-terminus of CDC20, creating a joint interface. In accordance with
 327 the X-ray structure, the R166 side chain of the CRY-box rotates towards the core of
 328 CDC20 through a stable interaction with the negatively charged residue E413 (2.7Å).
 329 This conformation of the CRY-box preserves a favorable docking interface for
 330 TCL1A. Substitution of R166 by alanine (CRY^{3A}) results in the loss of the stabilizing
 331 salt bridge, thereby weakening the TCL1A-CDC20 interaction (**Supplemental Figure**
 332 **7F**).

333 The HADDOCK 2.2 algorithm predicted two models that involve interactions of key
 334 aa of TCL1A (E9, E40, K42, R93, Y96), which are prone to form hydrogen bonds (or
 335 salt bridges) with respective residues of CDC20 (K440, E438, D173, Y167; **Figure**
 336 **6F, Supplemental Table 12**). The predicted residues of TCL1A would get in close
 337 proximity to the aa CRY165-167 of CDC20. The residues E40, K42, Y96 of TCL1A
 338 are expected to stabilize the TCL1A-CDC20 interaction in Model A, while E9, R93,
 339 Y96 would promote this interaction in Model B. For each model, HADDOCK statistics
 340 are displayed in **Supplemental Table 13**. To validate these *in-silico* models, we
 341 generated two TCL1A mutants fused to a FLAG-tag and stably overexpressed them
 342 in JVM3 cells: (1) EKY^{SAE}: E40S, K42A, Y96E (Model A) and (2) ERY^{KDE}: E9K,
 343 R93D, Y96E (Model B) (**Figure 6G**). The ERY^{KDE} aa substitutions did not affect the
 344 TCL1A-CDC20 interaction, while EKY^{SAE} nearly abolished it, supporting *in-silico*
 345 Model A. Overall, these *in-silico* models together with the IP data on CDC20 and
 346 TCL1A mutants confirm and provide the structural basis for the direct TCL1A-CDC20
 347 interaction. This, in turn, corroborates the concept of a modulatory impact of TCL1A
 348 on the activity of the MCC and/or APC/C during mitotic progression.

349 **TCL1A impairs the interaction of CDC20 with MAD2 and PLK1**

350 As MAD2 binding to CDC20 is crucial for a productive mitotic checkpoint,⁴³ we ana-
 351 lyzed the influence of TCL1A on the CDC20-MAD2 interaction in mitotic MEC1 and

352 HG3 cells (each -/+ TCL1A) via PLAs. There was a pronounced decrease in detected
353 CDC20-MAD2 interactions in both TCL1A-high lines compared to the respective con-
354 trol cells (**Figure 6H**), which was validated in JVM3 cells via co-IPs (**Supplemental**
355 **Figure 7G**). Next to the sequestration of CDC20 by MAD2, its binding to the APC/C
356 is negatively regulated via phosphorylation by PLK1.⁴⁴ In CDC20 co-IPs in JVM3
357 cells released from G2, we detected faster decreases of CDC20-PLK1 interactions
358 already 1h after release when TCL1A was present (**Figure 6I**), suggesting a TCL1A-
359 mediated impaired negative regulation of CDC20 by PLK1. Together, this defines a
360 novel molecular mechanism on the modulatory impact of TCL1A on the proficiency of
361 the mitotic checkpoint by impairing the interaction of CDC20 with its negative regula-
362 tors.

363 **Lower CDC20 expression correlates with features of aggressive CLL**

364 Besides this novel interaction of TCL1A with CDC20, there had been no reports on
365 CDC20 in CLL in general. *CDC20* was no target for mutations or copy number altera-
366 tions (CNAs) in large CLL series (CNA: N=319 CLL²⁹; mutations: N=1308 CLL, cBi-
367 oPortal⁴⁵⁻⁴⁸). We, therefore, analyzed its mRNA expression using publicly available
368 gene expression databases⁴⁹ and identified a pronounced *CDC20* downregulation
369 that was specific to CLL among several hematopoietic neoplasms (**Figure 7A**). At
370 the protein level, we detected lower CDC20 in the more aggressive U-CLL in com-
371 parison to M-CLL, which inversely correlated with TCL1A expression (**Figure 7B**).

372 This negative correlation was confirmed in GEP of patients included in the prospec-
373 tive CLL8 trial, which compared the outcome after fludarabine/cyclophosphamide
374 treatment with or without rituximab (FC vs FCR, **Figure 7C**).²⁷ The expression of
375 *CDC20* and *TCL1A* correlated with levels of key DDR and cell-cycle regulating
376 genes, including *ATM* and *TP53* (**Supplemental Figure 8A-C**). Significantly higher
377 WBC counts were observed in the *CDC20*-low group (median 101.3 vs 78.4 G/L for
378 low vs high *CDC20* levels; *P*=0.003; **Figure 7D**). Moreover, in univariate analyses,
379 low *CDC20* expression was associated with shorter progression-free survival (PFS)
380 of patients in the FC arm of the trial (median 25.5 vs 34.1 months for low vs high
381 *CDC20*; *P*=0.014; **Figure 7E, Supplemental Table 14**). As no effect on PFS was
382 observed for patients in the FCR arm (**Supplemental Figure 8D**), it is tempting to
383 speculate that a *CDC20* effect is overridden by the impact of the immunotherapeutic
384 component R, which targets much less cell-cycle dependent than classical chemo-
385 therapy (i.e. FC).

386 Moreover, in CLL subgroups that we previously defined by their molecular profiles²⁹,
387 *CDC20* expression was significantly lower in those cases that carry a 'genome insta-

388 bility' signature ($p<0.001$, **Figure 7F**). Together, CDC20 shows a specific downregulation
 389 in CLL and lower levels mark a more aggressive genomically instable disease.

390 **Low CDC20 expression is a feature of aggressive *E μ -TCL1A* cell populations**

391 As in CLL samples, we also detected a reduced CDC20 protein expression in spleenocytes of *E μ -TCL1A* mice as compared to those from *wt* animals (**Supplemental**
 392 **Figure 9A**). To assess the association of reduced *CDC20* expression with characteristics
 393 of cellular subsets, we made use of our previously published single-cell RNA
 394 sequencing (scRNA-seq) data from *E μ -TCL1A* mice and its derived allele *E μ -*
 395 *TCL1A^{Akt-C}*, which resembles aggressive Richter's transformation.³⁰ Integrative analysis
 396 of transcriptomes of cells from both models identified eight B-cell clusters, of
 397 which two were predominantly enriched in *E μ -TCL1A* mice (cluster 2, 10), while six
 398 were enriched in *E μ -TCL1A^{Akt-C}* or shared with *E μ -TCL1A* mice (cluster 0, 3, 13, 18,
 399 19, 20; **Figure 7G, Supplemental Table 15**). In *E μ -TCL1A* mice, *Cdc20* expression
 400 was confined to the dominant cluster 2 (**Figure 7H**). In those *E μ -TCL1A* B-cells clustering
 401 with the more aggressive *E μ -TCL1A^{Akt-C}* B-cells, hardly any *Cdc20* expression
 402 was detected. Differential gene expression analysis of the *Cdc20*-high vs all other
 403 clusters (*Cdc20*-low) identified 746 significant genes, of which most were upregulated
 404 in the *Cdc20*-high cluster. Consequently, most gene ontology processes were
 405 defined by genes upregulated in the *Cdc20*-high cluster (**Supplemental Figure 9B-D, Supplemental Tables 16-17**). In line with the patient data, *TCL1A* expression
 406 was higher in the *Cdc20*-negative clusters (**Figure 7I, Supplemental Table 16**; $P<0.001$). These data further confirm more aggressive characteristics of cells with
 407 low *CDC20* expression.

411 **CDC20 ablation accelerates leukemic outgrowth in mice**

412 To validate the impact of modulated *Cdc20* on murine CLL, we created from an *E μ -*
 413 *TCL1A* transplantable mouse model⁵⁰ a version with shRNA-mediated *Cdc20* knock-
 414 down (*E μ -TCL1A;Cdc20-KD*, **Figure 7J**). At the early disease stage, a significantly
 415 faster outgrowth of Cd5+/Cd19+ B-cells was observed in recipients transplanted with
 416 *E μ -TCL1A;Cdc20-KD* cells (N=15) as compared to mice transplanted with cells con-
 417 taining a GFP-coupled scramble shRNA vector (*E μ -TCL1A;GFP*; N=19; **Figure 7K**).
 418 The shorter survival of *E μ -TCL1A;Cdc20-KD* mice was statistically not significant,
 419 likely due to the highly aggressive character of the disease model (**Supplemental**
 420 **Figure 10A**). Slightly elevated cyclin D1 levels ($P=0.01$) and reduced PARP cleavage
 421 ($P=0.048$) were seen in *E μ -TCL1A;Cdc20-KD* mice indicating higher proliferation
 422 rates and apoptotic resistance (**Figure 7L, Supplemental Figure 10B**). This was
 423 paralleled by slightly elevated levels of pAkt and Bcl2 in *E μ -TCL1A;Cdc20-KD* cells

424 (**Supplemental Figure 10C**). *Eμ-TCL1A;Cdc20-KD* tumors also acquired a signifi-
425 cantly higher proportion of aneuploidy ($P=0.014$) as compared to *Eμ-TCL1A;GFP*
426 cells (**Figure 7M**).

427 **Discussion**

428 Although TCL1A is established to centrally contribute to T-cell and B-cell lym-
429 phomagenesis, the molecular concept of, particularly nuclear, TCL1A effectors and
430 target pathways has remained incomplete. The majority of described TCL1A-
431 interacting proteins can be assigned to the governance of cell survival.^{13–15,51,52} Sin-
432 gle-gene targeting of particular TCL1A executioners, i.e. AKT1 or ATM, however,
433 does not reproduce the phenotype of TCL1A-driven tumors.^{17,53} Therefore, the spec-
434 trum of molecular and cell-biological consequences of TCL1A dysregulation as well
435 as the contexts (cell type, stimuli) in which such TCL1A-target engagements occur,
436 are not fully represented by its recognized effectors.¹⁸ Our animal experiments here
437 implicate particularly nuclear TCL1A to be of highly transforming potential.

438 The present study provides first evidence for a modulating effect of TCL1A on mitotic
439 progression and identifies a new and unique nuclear protein spectrum engaged by
440 TCL1A. Through multiple proteomic analyses, we demonstrate that TCL1A interacts
441 with a range of proteins that orchestrate DDR pathways, particularly cell cycle
442 checkpoints. The ‘cell cycle’ was one of the most prominent functional clusters en-
443 riched in the TCL1A interactome and its key regulatory molecules such as CDC20,
444 CDK1, or MAD2 colocalized with TCL1A in the cytoplasm and at the mitotic spindle.

445 The observed cellular consequences of (enforced) TCL1A expression in several
446 CLL-like cell lines⁵⁴ and in *Eμ-TCL1A* mice, i.e. an accelerated entry and transition
447 through mitosis, corroborate these molecular findings. Further in line with this new
448 mode of TCL1A’s action, a higher rate of aneuploidy coincided with a higher inci-
449 dence of multipolar spindles and aberrant responses to DNA damage. The primary
450 occurrence of aneuploidy in pre-leukemic *Eμ-TCL1A* mice indicates a direct TCL1A
451 effect rather than this being a secondary phenomenon of tumor progression.

452 At the core of our findings, we established a direct physical interaction of TCL1A with
453 the APC/C cofactor CDC20. In contrast to its interaction with AKT⁴⁰, a disrupted di-
454 merization of TCL1A did not influence TCL1A-CDC20 complex formation, suggesting
455 that TCL1A interacts with CDC20 prior to its homo-dimerization or that interaction of
456 CDC20 with monomeric TCL1A is functionally sufficient. Through a combined bio-
457 chemical and *in-silico* modeling approach, we defined the crucial regions of the
458 TCL1A-CDC20 interaction with the aa E40, K42, and Y96 of TCL1A as well as the
459 MIM and CRY boxes of CDC20, which are important degrons in regulating the MCC-
460 to-APC/C switch.^{23,55} Therefore, our structure-based predictions suggest a functional
461 consequence of TCL1A-bound CDC20 on the MCC and/or APC/C. Indeed, we identi-
462 fied a TCL1A-associated disrupted interaction of CDC20 with its negative regulators

463 MAD2 (sequestration of CDC20 by the MCC²³) and PLK1 (inhibitory
464 phosphorylation⁴⁴). These data imply TCL1A to perturb proper mitotic checkpoint
465 function, likely contributing to accelerated cell cycle transition and accumulating an-
466 euploidy.

467 Is potentially tumor-suppressive CDC20 relevant in CLL? We observed a strong CLL-
468 specific transcriptional *CDC20* downregulation, which correlated inversely with
469 *TCL1A* expression. Lower expression of *CDC20* in CLL was associated with higher
470 genomic instability. Patients with *CDC20*-low CLL had a shorter PFS after chemo-
471 therapy. Lower *CDC20* is likely part of transcriptional programs of the more aggres-
472 sive *TCL1A*-high subset of U-CLL. Nevertheless, we demonstrated a rather direct
473 causal pro-leukemic impact of reduced *CDC20* in the context of *TCL1A* overexpres-
474 sion by experimental *Cdc20* downmodulation, which accelerated leukemic progres-
475 sion and higher rates of aneuploidy in the *Eμ-TCL1A* CLL model. At the single-cell
476 level of *TCL1A*-induced murine CLL, *Cdc20*-low/negative clusters showed highest
477 *TCL1A* expression and were associated with a more aggressive phenotype, e.g. in
478 our model of Richter's transformation. Interestingly and in contrast to our observa-
479 tions in CLL, higher levels of *CDC20* in solid tumors (normally *TCL1A* negative) are
480 associated with treatment resistance, dissemination, and poor prognosis.^{56–58} Such a
481 particular dual relationship of a *TCL1A* target protein and down-regulated safeguard-
482 ing molecule is shown already for the *TCL1A*-ATM interaction.^{2,4,51}

483 Overall, our findings add valuable new insights to the molecular concept of, thus far
484 underappreciated nuclear, executioners of oncogenic *TCL1A*. We conclude that
485 *TCL1A* overexpression promotes premature, DNA-damage-prone cell cycle check-
486 point transition, which in context-specific synergy with impaired damage repair and
487 hyperactive pro-survival signaling (**visual abstract**) mediates the transforming im-
488 pact of *TCL1A*. This provides a rationale for more informed targeting strategies.

489 **Acknowledgements**

490 CLL sample acquisition was supported by the Biobank of the CIO ABCD funded by
491 the German Cancer Aid. The analysis of GEP data of the CLL8 trial was supported
492 by the German CLL Study Group. We thank S. Michnick (University of Montreal,
493 Canada) for the provision of constructs. Mass spectrometry analyses were conduct-
494 ed at the CECAD proteomics facility. Use of Olympus microscopes was provided by
495 the microscopy core facility of the Cologne Center for Genomics (CMMC, Germany).
496 Sample processing and single-cell RNA sequencing was performed by M. Franitz,
497 J. Altmüller, and T. Georgomanolis (CMMC, Germany). Pre-processing of single-cell
498 RNA sequencing data was performed by M. Nikolic and M. Peifer (CMMC, Germa-
499 ny). M. Herling (PI) and E. Vasyutina (female research grant) receive support from
500 the German Research Foundation (DFG, HE-3553/3-2) as part of the collaborative
501 research group KFO-286. M. Herling was funded by the José Carreras Leukemia
502 Foundation (R12/08) and the DFG Research Unit FOR1961 (Control-T; HE3553/4-2).
503 E. Vasyutina received financial support from Köln Fortune Program (110/2012),
504 German Cancer Aid (70112788), Nolting, Kaethe-Hack, and Hochhaus Foundations.
505 CMMC Program (Project C08; Project 23-RP, to M. Herling and E. Vasyutina) has
506 also funded this project.

507

508 **Authorship contributions**

509 E. Vasyutina, J. Stachelscheid, Q. Jiang, C. Aszyk, M. Hallek, S. Stilgenbauer, J.
510 Bloehdorn, and M. Herling designed the experiments and analyzed the *in-vitro* gen-
511 erated data. E. Vasyutina, J. Stachelscheid, C. Aszyk, Q. Jiang, T. Müller, O.
512 Vydzhak, K. Symeonidis, and P. Mayer performed the *in-vitro* experiments. E.
513 Vasyutina, K. Warner, G. Crispatzu, and S. Newrzela designed, performed, and ana-
514 lyzed the *in vivo* experiments and GEP data of mice. MS experiments and statistical
515 analyses were performed by M. Krueger, J. Stachelscheid and C. Aszyk. G.
516 Goehring, S. Hippler, and K.A. Kreuzer performed cytogenetic analyses. A. Lechner
517 and D. Beutner acquired human tissue samples. N. Bley and S. Hüttelmaier per-
518 formed PLA experiments. J. Bloehdorn, S. Robrecht, K. Fischer, and S. Stilgenbauer
519 acquired and analyzed GEP and clinical data of the CLL8 trial, S.J. Blakemore and
520 C. Pallasch performed scRNA-seq data analysis, D. Auguin performed the molecular
521 modelling and the *in-silico* analysis of protein complexes. E. Vasyutina, J.
522 Stachelscheid, and M. Herling wrote the manuscript.

523

524 **Conflict of interest disclosure**

525 The authors declare no competing financial interests.

526 **References**

- 527 1. Virgilio L, Narducci MG, Isobe M, et al. Identification of the TCL1 gene
528 involved in T-cell malignancies. *Proc. Natl. Acad. Sci. U. S. A.*
529 1994;91(26):12530–4.
- 530 2. Schrader A, Crispatzu G, Oberbeck S, et al. Actionable perturbations of
531 damage responses by TCL1/ATM and epigenetic lesions form the basis of T-
532 PLL. *Nat. Commun.* 2018;9(1):697.
- 533 3. Pekarsky Y, Zanesi N, Croce CM. Molecular basis of CLL. *Semin. Cancer Biol.*
534 2010;20(6):370–376.
- 535 4. Herling M, Patel KA, Khalili J, et al. TCL1 shows a regulated expression
536 pattern in chronic lymphocytic leukemia that correlates with molecular
537 subtypes and proliferative state. *Leukemia.* 2006;20(2):280–285.
- 538 5. Herling M, Patel KA, Teitell MA, et al. High TCL1 expression and intact T-cell
539 receptor signaling define a hyperproliferative subset of T-cell prolymphocytic
540 leukemia. *Blood.* 2008;111(1):328–37.
- 541 6. Herling M, Patel KA, Weit N, et al. High TCL1 levels are a marker of B-cell
542 receptor pathway responsiveness and adverse outcome in chronic
543 lymphocytic leukemia. *Blood.* 2009;114(21):4675–86.
- 544 7. Hopfinger G, Busch R, Pflug N, et al. Sequential chemoimmunotherapy of
545 fludarabine, mitoxantrone, and cyclophosphamide induction followed by
546 alemtuzumab consolidation is effective in T-cell prolymphocytic leukemia.
547 *Cancer.* 2013;119(12):2258–67.
- 548 8. Ramuz O, Bouabdallah R, Devilard E, et al. Identification of TCL1A as an
549 immunohistochemical marker of adverse outcome in diffuse large B-cell
550 lymphomas. *Int. J. Oncol.* 2005;26(1):151–7.
- 551 9. Herling M, Patel KA, Hsi ED, et al. TCL1 in B-cell tumors retains its normal b-
552 cell pattern of regulation and is a marker of differentiation stage. *Am. J. Surg.
553 Pathol.* 2007;31(7):1123–9.
- 554 10. Aggarwal M, Villuendas R, Gomez G, et al. TCL1A expression delineates
555 biological and clinical variability in B-cell lymphoma. *Mod. Pathol.*
556 2009;22(2):206–15.
- 557 11. Virgilio L, Lazzeri C, Bichi R, et al. Deregulated expression of TCL1 causes T
558 cell leukemia in mice. *Proc. Natl. Acad. Sci. U. S. A.* 1998;95(7):3885–9.
- 559 12. Bichi R, Shinton SA, Martin ES, et al. Human chronic lymphocytic leukemia
560 modeled in mouse by targeted TCL1 expression. *Proc. Natl. Acad. Sci. U. S.
561 A.* 2002;99(10):6955–60.
- 562 13. Pekarsky Y, Koval A, Hallas C, et al. Tcf1 enhances Akt kinase activity and
563 mediates its nuclear translocation. *Proc. Natl. Acad. Sci. U. S. A.*
564 2000;97(7):3028–33.
- 565 14. Laine J, Künstle G, Obata T, Sha M, Noguchi M. The protooncogene TCL1 is
566 an Akt kinase coactivator. *Mol. Cell.* 2000;6(2):395–407.
- 567 15. Pekarsky Y, Palamarchuk A, Maximov V, et al. Tcf1 functions as a
568 transcriptional regulator and is directly involved in the pathogenesis of CLL.
569 *Proc. Natl. Acad. Sci. U. S. A.* 2008;105(50):19643–8.
- 570 16. Oberbeck S, Schrader A, Warner K, et al. Noncanonical effector functions of
571 the T-memory-like T-PLL cell are shaped by cooperative TCL1A and TCR
572 signaling. *Blood.* 2020;136(24):2786–2802.

- 573 17. Kharas MG, Okabe R, Ganis JJ, et al. Constitutively active AKT depletes
 574 hematopoietic stem cells and induces leukemia in mice. *Blood*.
 575 2010;115(7):1406–15.
- 576 18. Stachelscheid J, Jiang Q, Herling M. The modes of dysregulation of the proto-
 577 oncogene T-cell leukemia/lymphoma 1A. *Cancers (Basel)*. 2021;13(21):5455.
- 578 19. Klein U, Lia M, Crespo M, et al. The DLEU2/miR-15a/16-1 cluster controls B
 579 cell proliferation and its deletion leads to chronic lymphocytic leukemia.
 580 *Cancer Cell*. 2010;17(1):28–40.
- 581 20. Kienle DL, Korz C, Hosch B, et al. Evidence for distinct pathomechanisms in
 582 genetic subgroups of chronic lymphocytic leukemia revealed by quantitative
 583 expression analysis of cell cycle, activation, and apoptosis-associated genes.
 584 *J. Clin. Oncol.* 2005;23(16):3780–92.
- 585 21. Decker T, Schneller F, Hipp S, et al. Cell cycle progression of chronic
 586 lymphocytic leukemia cells is controlled by cyclin D2, cyclin D3, cyclin-
 587 dependent kinase (cdk) 4 and the cdk inhibitor p27. *Leukemia*.
 588 2002;16(3):327–34.
- 589 22. Schmidt M, Rohe A, Platzer C, et al. Regulation of G2/M Transition by
 590 Inhibition of WEE1 and PTKMYT1 Kinases. *Molecules*. 2017;22(12):2045.
- 591 23. Chao WCH, Kulkarni K, Zhang Z, Kong EH, Barford D. Structure of the mitotic
 592 checkpoint complex. *Nature*. 2012;484(7393):208–13.
- 593 24. Vleugel M, Hoogendoorn E, Snel B, Kops GJPL. Evolution and function of the
 594 mitotic checkpoint. *Dev. Cell*. 2012;23(2):239–50.
- 595 25. Fedorchenko O, Stiefelhagen M, Peer-Zada AA, et al. CD44 regulates the
 596 apoptotic response and promotes disease development in chronic lymphocytic
 597 leukemia. *Blood*. 2013;121(20):4126–36.
- 598 26. Newrzela S, Cornils K, Li Z, et al. Resistance of mature T cells to oncogene
 599 transformation. *Blood*. 2008;112(6):2278–86.
- 600 27. Hallek M, Fischer K, Fingerle-Rowson G, et al. Addition of rituximab to
 601 fludarabine and cyclophosphamide in patients with chronic lymphocytic
 602 leukaemia: a randomised, open-label, phase 3 trial. *Lancet (London, England)*.
 603 2010;376(9747):1164–74.
- 604 28. Vasyutina E, Boucas JM, Bloehdorn J, et al. The regulatory interaction of EVI1
 605 with the TCL1A oncogene impacts cell survival and clinical outcome in CLL.
 606 *Leukemia*. 2015;29(10):2003–14.
- 607 29. Bloehdorn J, Braun A, Taylor-Weiner A, et al. Multi-platform profiling
 608 characterizes molecular subgroups and resistance networks in chronic
 609 lymphocytic leukemia. *Nat. Commun.* 2021;12(1):5395.
- 610 30. Kohlhaas V, Blakemore SJ, Al-Maarri M, et al. Active Akt signaling triggers
 611 CLL toward Richter transformation via overactivation of Notch1. *Blood*.
 612 2021;137(5):646–60.
- 613 31. Perez-Riverol Y, Csordas A, Bai J, et al. The PRIDE database and related
 614 tools and resources in 2019: improving support for quantification data. *Nucleic
 615 Acids Res.* 2019;47(D1):D442–D450.
- 616 32. Sancar A, Lindsey-Boltz LA, Unsal-Kaçmaz K, Linn S. Molecular mechanisms
 617 of mammalian DNA repair and the DNA damage checkpoints. *Annu. Rev.
 618 Biochem.* 2004;73(1):39–85.
- 619 33. Bailis JM, Forsburg SL. MCM proteins: DNA damage, mutagenesis and repair.
 620 *Curr. Opin. Genet. Dev.* 2004;14(1):17–21.

- 621 34. Kaneta Y, Ullrich A. NEK9 depletion induces catastrophic mitosis by
622 impairment of mitotic checkpoint control and spindle dynamics. *Biochem.*
623 *Biophys. Res. Commun.* 2013;442(3–4):139–46.
- 624 35. Lara-Gonzalez P, Moyle MW, Budrewicz J, et al. The G2-to-M Transition Is
625 Ensured by a Dual Mechanism that Protects Cyclin B from Degradation by
626 Cdc20-Activated APC/C. *Dev. Cell.* 2019;51(3):313–325.e10.
- 627 36. Michnick SW, Ear PH, Landry C, Malleshaiah MK, Messier V. Protein-
628 Fragment Complementation Assays for Large-Scale Analysis, Functional
629 Dissection and Dynamic Studies of Protein–Protein Interactions in Living Cells.
630 *Methods Mol. Biol.* 2011;756:395–425.
- 631 37. Pfleger CM, Lee E, Kirschner MW. Substrate recognition by the Cdc20 and
632 Cdh1 components of the anaphase-promoting complex. *Genes Dev.*
633 2001;15(18):2396–407.
- 634 38. Labit H, Fujimitsu K, Bayin NS, et al. Dephosphorylation of Cdc20 is required
635 for its C-box-dependent activation of the APC/C. *EMBO J.* 2012;31(15):3351–
636 62.
- 637 39. Ge S, Skaar JR, Pagano M. APC/C- and Mad2-mediated degradation of
638 Cdc20 during spindle checkpoint activation. *Cell Cycle.* 2009;8(1):167–71.
- 639 40. Auguin D, Barthe P, Royer C, et al. Structural basis for the co-activation of
640 protein kinase B by T-cell leukemia-1 (TCL1) family proto-oncoproteins. *J.*
641 *Biol. Chem.* 2004;279(34):35890–902.
- 642 41. Dominguez C, Boelens R, Bonvin AMJJ. HADDOCK: a protein-protein docking
643 approach based on biochemical or biophysical information. *J. Am. Chem. Soc.*
644 2003;125(7):1731–7.
- 645 42. Dosztányi Z, Csizmok V, Tompa P, Simon I. IUPred: web server for the
646 prediction of intrinsically unstructured regions of proteins based on estimated
647 energy content. *Bioinformatics.* 2005;21(16):3433–4.
- 648 43. Izawa D, Pines J. Mad2 and the APC/C compete for the same site on Cdc20
649 to ensure proper chromosome segregation. *J. Cell Biol.* 2012;199(1):27–37.
- 650 44. Jia L, Li B, Yu H. The Bub1–Plk1 kinase complex promotes spindle checkpoint
651 signalling through Cdc20 phosphorylation. *Nat. Commun.* 2016;7(1):10818.
- 652 45. Landau DA, Carter SL, Stojanov P, et al. Evolution and impact of subclonal
653 mutations in chronic lymphocytic leukemia. *Cell.* 2013;152(4):714–26.
- 654 46. Landau DA, Tausch E, Taylor-Weiner AN, et al. Mutations driving CLL and
655 their evolution in progression and relapse. *Nature.* 2015;526(7574):525–30.
- 656 47. Quesada V, Conde L, Villamor N, et al. Exome sequencing identifies recurrent
657 mutations of the splicing factor SF3B1 gene in chronic lymphocytic leukemia.
658 *Nat. Genet.* 2011;44(1):47–52.
- 659 48. Puente XS, Beà S, Valdés-Mas R, et al. Non-coding recurrent mutations in
660 chronic lymphocytic leukaemia. *Nature.* 2015;526(7574):519–24.
- 661 49. Haferlach T, Kohlmann A, Wieczorek L, et al. Clinical utility of microarray-
662 based gene expression profiling in the diagnosis and subclassification of
663 leukemia: report from the International Microarray Innovations in Leukemia
664 Study Group. *J. Clin. Oncol.* 2010;28(15):2529–37.
- 665 50. Suljagic M, Longo PG, Bennardo S, et al. The Syk inhibitor fostamatinib
666 disodium (R788) inhibits tumor growth in the Eμ- TCL1 transgenic mouse
667 model of CLL by blocking antigen-dependent B-cell receptor signaling. *Blood.*
668 2010;116(23):4894–905.

- 669 51. Gaudio E, Spizzo R, Paduano F, et al. Tcf1 interacts with Atm and enhances
670 NF-κB activation in hematologic malignancies. *Blood*. 2012;119(1):180–7.
- 671 52. Sivina M, Hartmann E, Vasyutina E, et al. Stromal cells modulate TCL1
672 expression, interacting AP-1 components and TCL1-targeting micro-RNAs in
673 chronic lymphocytic leukemia. *Leukemia*. 2012;26(8):1812–20.
- 674 53. Barlow C, Hirotsune S, Paylor R, et al. Atm-deficient mice: a paradigm of
675 ataxia telangiectasia. *Cell*. 1996;86(1):159–71.
- 676 54. Lanemo Myhrinder A, Hellqvist E, Bergh A-C, et al. Molecular characterization
677 of neoplastic and normal “sister” lymphoblastoid B-cell lines from chronic
678 lymphocytic leukemia. *Leuk. Lymphoma*. 2013;54(8):1769–1779.
- 679 55. Yamaguchi M, VanderLinden R, Weissmann F, et al. Cryo-EM of Mitotic
680 Checkpoint Complex-Bound APC/C Reveals Reciprocal and Conformational
681 Regulation of Ubiquitin Ligation. *Mol. Cell*. 2016;63(4):593–607.
- 682 56. Wang S, Chen B, Zhu Z, et al. CDC20 overexpression leads to poor prognosis
683 in solid tumors: A system review and meta-analysis. *Medicine (Baltimore)*.
684 2018;97(52):e13832.
- 685 57. Alfarsi LH, Ansari R El, Craze ML, et al. CDC20 expression in oestrogen
686 receptor positive breast cancer predicts poor prognosis and lack of response
687 to endocrine therapy. *Breast Cancer Res. Treat.* 2019;178(3):535–44.
- 688 58. Song C, Lowe VJ, Lee S. Inhibition of Cdc20 suppresses the metastasis in
689 triple negative breast cancer (TNBC). *Breast Cancer*. 2021;28(5):1073–86.
- 690 59. de Vries SJ, Bonvin AMJJ. CPoRT: a consensus interface predictor and its
691 performance in prediction-driven docking with HADDOCK. *PLoS One*.
692 2011;6(3):e17695.
- 693

694 **Figure legends**

695 **Visual abstract.**

696 **Proposed integrative model of oncogenic TCL1A through the promotion of ge-**
697 **nomic instability in malignant B-cells.**

698 Overexpression of TCL1A causes genomic instability via multiple pathways: (i) defi-
699 cient repair of DNA damage, (ii) an accelerated cell cycle transition, (iii) susceptibility
700 to aneuploidy (data for i-iii presented in this report), and (iv) apoptosis resistance
701 (published before). Key molecules through which these effects (i.e. via physical in-
702 teraction with TCL1A) are mediated are highlighted. We show here that overexpres-
703 sion of TCL1A leads to a decreased phosphorylation of ATM and reduced expression
704 of p53 upon genotoxic stress. This might cause impaired sensing and processing of
705 DNA insults (exogeneous or as part of DNA replication), and deficient G2/M check-
706 point control, contributing to (i) and (ii). The interaction of TCL1A with molecules from
707 the mitotic checkpoint complex (MCC), including CDC20, might form the basis of the
708 observed accelerated cell cycle transition by deregulating the mitotic checkpoint,
709 contributing to (ii) and (iii). Furthermore, the high frequency of aberrant spindles seen
710 in TCL1A-overexpressing cells promotes the observed aneuploidy. The already well-
711 established role of TCL1A in augmenting AKT phosphorylation^{6,13,16} leads to in-
712 creased survival signaling and thereby to apoptotic resistance (perturbation of a
713 safeguarding mechanism). Together, TCL1A overexpression leads to a premature,
714 DNA-damage-prone cell cycle checkpoint transition, which contributes to the TCL1A
715 transforming capability in concert with impaired repair and hyperactive pro-survival
716 signaling.

717 **Figure 1. Pronounced oncogenic function of nuclear TCL1A.**

718 **(A)** Experimental setup of adoptive transfer of human (h)TCL1A transgenic stem
719 cells: HSC/HPC, isolated from B6.SJL donor mice were retrovirally transduced with
720 vectors expressing different variants of human TCL1A (bottom). hTCL1A: unrestrict-
721 ed wild-type TCL1A; myr-hTCL1A: membrane-targeted TCL1A expression; nls-
722 hTCL1A: nuclear enrichment of TCL1A. After transduction, cells were injected into
723 bone-marrow-depleted C57BL/6 mice. **(B)** Immunofluorescence images of HEK293T
724 cells retrovirally transduced with three different TCL1A variants, validating their sub-
725 cellular localization. Images were captured at 60x magnification using an Axio
726 Scope.A1 fluorescent microscope (Zeiss, Germany). For subcellular distribution of
727 TCL1A in the lymphomatous spleens see **Supplemental Figure 1B**. **(C)** Kaplan-
728 Meier curves of mice transplanted with HSC/HPC, expressing generic hTCL1A
729 (black, N=5), myr-hTCL1A (blue, N=16), and nls-hTCL1A (red, N=15). Log-rank-test
730 showed a significantly shorter survival of nls-hTCL1A in comparison to hTCL1A re-
731 cipient mice. For an overview of disease characteristics of transplanted mice see
732 **Supplemental Table 1** and for histology of organs see **Supplemental Figure 1C**.
733 **(D)** Gene expression of splenocytes from mice with B-cell malignancies (>70% tumor
734 cell content) was analyzed via microarrays. GSEA identified several deregulated
735 pathways between lymphomas of nls-hTCL1A vs hTCL1A recipient mice (*FDR*
736 <0.05). Identified nuclear pathways are upregulated in tumor cells from nls-hTCL1A
737 recipients. Deregulated pathways for TCL1A variants vs GFP only and myr-hTCL1a
738 vs nls-TCL1A are displayed in **Supplemental Figure 2**. **(E)** Enrichment plots of sig-
739 nificantly deregulated pathways involved in cell cycle and in DNA repair between nls-
740 hTCL1A- and hTCL1A-expressing cells.

741 **Figure 2. Proteins involved in the DNA repair and the cell cycle pathways are**
742 **common interaction partners of TCL1A.**

743 **(A)** Experimental setup: TCL1A co-immunoprecipitations (co-IPs) were performed
744 from lysates of primary CLL cells, divided into two subgroups based on their IGHV
745 gene mutation status. Primary B-cells isolated from tonsils were used as healthy con-
746 trols (N=3). Co-IPs with IgG served as a negative control (N=3 CLL lysates). Pro-
747 cessed immunoprecipitates were analyzed on an LFQ LC-MS/MS device. **(B)** Venn
748 diagrams showing the overlap of identified TCL1A-interacting proteins between
749 healthy B-cells from tonsils and CLL cells, as well as between U-CLL and M-CLL (for
750 the comparison of cytogenetic/clinical risk groups “no go” vs. “slow go” vs. “high-risk”
751 see **Supplemental Figure 3**. Proteins were considered interactors when they were
752 significantly enriched in the corresponding group vs IgG control (FDR q-value <0.05,
753 FCh >2, Welch-test). **(C)** Overview of enriched pathway clusters within the TCL1A
754 interactome identified by over-representation analysis (ORA) using the Cytoscape
755 plug-in ClueGO (v2.5.8, Reactome database), indicating the percentage of terms per
756 cluster. **Supplemental Figure 4** shows the associated functional networks of all en-
757 riched pathways identified by ClueGO. **(D)** Bar graph of selected pathways identified
758 in (C) illustrating the percentage of associated proteins from the TCL1A interactome
759 within each pathway. **(E-F)** Heat map of TCL1A interactors belonging to (E) the cell
760 cycle pathway and (F) the DNA repair pathway as identified by ORA using ClueGO.

761 **Figure 3. Systematic mass-spectrometry based analysis of TCL1A interacting**
762 **partners identifies mitotic checkpoint regulators.**

763 **(A)** Experimental setup: TCL1A-bound protein complexes were isolated from JVM3
764 CLL-like cells +/- transfected TCL1A; at baseline (untreated culture), under genotoxic
765 stress (5 μ M etoposide for 4.5h), or synchronized in mitosis (100 ng/ml nocodazole
766 for 18h, release for 1h), followed by LFQ LC-MS/MS mass spectrometry (MS). **(B)**
767 MS identified in total 962 significantly TCL1A-interacting proteins (cut-offs per group:
768 FDR q-value <0.05, FCh>2; Student's t-test). Most proteins differentially interact with
769 TCL1A in JVM3^{TCL1A} B-cells only at baseline (blue) or under genotoxic stress (yellow)
770 or during mitosis (green). **(C)** Overview of enriched pathway clusters within the
771 TCL1A interactome identified by over-representation analysis (ORA) using Cyto-
772 scape plug-in ClueGO (v2.5.8). Enriched pathways highly depend on the condition.
773 **(D)** Overview of selected enriched pathways (Reactome pathway database) within
774 the TCL1A interactome identified in (C). **(E)** STRING network of TCL1A interactors
775 involved in the cell cycle checkpoint of JVM3 cells under genotoxic stress (left) and
776 synchronized in mitosis (right) identified by ClueGO. Colors indicate the involvement
777 in the particular cell cycle checkpoint (green: G1/S transition, blue: G2/M checkpoint,
778 red: separation of sister chromatids, yellow: inhibition of APC/C via direct inhibition of
779 the APC/C complex). Note the marked network expansion upon mitosis induction.
780 Mitotic checkpoint proteins (e.g. CDC20, MAD2, and CDC27, a subunit of the APC/C
781 E3 ubiquitin ligase complex) appear centrally involved in TCL1A signaling in mitosis
782 only.

783 **Figure 4. *TCL1A* overexpression leads to aberrant cell cycle progression.**

784 **(A)** Immunoblots of co-Immunoprecipitations (co-IPs) of B-cells from spleens of *wt* or
785 *E μ -TCL1A* mice using anti-TCL1A antibodies or isotype IgG (negative control). Lanes
786 represent individual animals. **(B)** Immunoblots of co-IPs using IgG controls or specific
787 *TCL1A* antibodies in primary CLL samples co-cultured with differentiated THP-1
788 monocytic cells in the presence of CpG and IL-15 for 36h to induce proliferation.
789 Lanes represent individual CLL samples. **(C)** Box plot showing percentages of cells
790 in G0/G1 (top) and G2/M (bottom) of JVM3 +/- *TCL1A* that were released from RO-
791 3306 synchronization from four independent experiments. Boxes display medians
792 with 25th-75th percentiles and whiskers of 5th-95th percentiles. Significances were es-
793 timated by the Mann-Whitney test. Analogous results for HEK293T and DoHH2 cells
794 (*TCL1A* introduction) as well as for MEC1 cells (shRNA-mediated *TCL1A* knock-
795 down) are shown in **Supplemental Figure 6A**. **(D)** Flow cytometric analysis of G2/M
796 synchronized (via RO-3306 for 20h) JVM3 cells +/- *TCL1A* stained with Hoechst.
797 Representative histogram shows an accelerated exit from the G2/M into the G1 cell
798 cycle phase after release in full medium of *TCL1A*-overexpressing cells. Grey:
799 JVM3^{empty vector (EV)}, blue: JVM3^{TCL1A}. **(E)** Representative immunoblot from lysates of
800 cells released from RO-3306-mediated synchronization. JVM3^{TCL1A} cells show faster
801 dephosphorylation of proteins involved in the regulation of cell cycle transition as well
802 as a faster degradation of Cyclin A and B, and CDC20. Analogous results for
803 HEK293T and DoHH2 cells (*TCL1A* transfection) as well as for MEC1 cells (*TCL1A*
804 knock-down) are in **Supplemental Figure 6B**. **(F)** Aberrant cell cycle progression in
805 *TCL1A*-driven murine leukemia. Top: *E μ -TCL1A* mice (N=4) or age-matched *wt* con-
806 trols (N=3) were injected with BrdU. At 20h post-injection, the ratios of BrdU+ (in S-
807 phase at time of injection, green), p-H3+ (in mitosis at time of harvest, red), BrdU+;p-
808 H3+ (formerly in S-phase, currently mitotic, yellow), and BrdU-;p-H3- (not proliferat-
809 ing, blue) cell counts were determined by immunostaining (2500 cells/animal; Stu-
810 dent's t-test). Images were captured at 60x magnification using an Axio Scope.A1
811 fluorescent microscope (Zeiss, Germany). Bottom: Increased overall proliferation (S-
812 phase and mitosis) of *E μ -TCL1A* cells (BrdU+ and p-H3+). These *TCL1A*-transgenic
813 cells exited the cell cycle more often (higher proportion of BrdU+;p-H3- and similar
814 proportion of BrdU+/p-H3+ cells). An increased population of BrdU-/p-H3+ cells in the
815 *E μ -TCL1A* cohort also suggests that they re-enter the cell cycle more frequently.

816 **Figure 5. TCL1A overexpression interferes with a proficient DNA-damage re-**
 817 **response and confers aneuploidy.**

818 **(A)** Immunoblot analysis of phosphorylated (p)ATM^{S1981} in freshly isolated CLL cells
 819 treated with 10μM etoposide for the indicated time points. Samples with low TCL1A
 820 expression (by qRT-PCR) show higher etoposide-induced phosphorylation and
 821 cleavage of ATM. **(B)** qRT-PCR analysis of *TCL1A* expression of patient samples
 822 from (A). **(C)** Top: Splenocytes from leukemic (10mo) *Eμ-TCL1A* mice showed a
 823 lower expression of p53 in comparison to age-matched *wt* mice. Bottom: TUNEL
 824 analysis of splenocytes from *wt* and *Eμ-TCL1A* mice shows more DNA breaks in
 825 *TCL1A* transgenic cells. Images at 60x magnification on an Axio Scope.A1 fluores-
 826 cent microscope (Zeiss, Germany). **(D)** JVM3 (N=5, representative photographs next
 827 to bar chart) and DoHH2 (N=4) cells, both +/- transgenic *TCL1A*, as well as MEC1
 828 cells (N=5; +/- shRNA-mediated *TCL1A* knock-down) were synchronized in G2 via
 829 treatment with 9μM RO-3306 for 20h. At 30min and 1h after release, the percentage
 830 of aberrant spindles was determined by immunohistochemistry; α-tubulin (green) and
 831 Hoechst (blue). The *TCL1A*-transgenic JVM3 and DoHH2 cells showed a more pro-
 832 nounced accumulation of multipolar spindles as compared to controls, which was
 833 reproduced in opposite direction in MEC1 cells after shRNA-mediated *TCL1A* knock-
 834 down. Range of 300-700 individual cells per condition; Student's t-test. Immunofluo-
 835 rescence images were captured at 60x magnification using an IX83 fluorescent mi-
 836 croscope (Olympus, Japan). **(E)** Flow-cytometric quantification of Hoechst staining in
 837 DoHH2 +/-*TCL1A* (top, N=3 per genotype) and JVM3 +/-*TCL1A* (bottom, N=5 per
 838 genotype). In both cell lines, increased DNA ploidy was found in the *TCL1A*-positive
 839 condition as compared to the respective control line. **(F)** G-banding-based karyotype
 840 analysis of DoHH2 +/-*TCL1A* B-cells. Comparison of representative karyograms of
 841 DoHH2-TCL1A (N=42) to DoHH2 parental cells (N=21) with a trend towards an in-
 842 creased genetic complexity (chromosome gains, losses, deletions, translocations) in
 843 the *TCL1A*-transfected cells. Percent of cells with genomic aberrations: DoHH2:
 844 14.3%; DoHH2-TCL1A: 23.8%; P=0.516, Fisher's exact test, quantification not illus-
 845 trated. **(G)** Spectral karyotyping (SKY) analysis of *Eμ-TCL1A* leukemic B-cells shows
 846 karyotypes with trisomies of chromosomes 15 and 19 and translocations of chromo-
 847 some 5. **(H)** Splenocytes from pre-leukemic (N=3, WBC <30x10⁶ cells/ml) or leuke-
 848 mic (N=5, WBC >50x10⁶ cells/ml) *Eμ-TCL1A* mice showed an aberrant number of
 849 chromosomes compared to *wt* (N=3) mice; Student's t-test.

850 **Figure 6. The interaction of TCL1A and CDC20 takes place via defined motifs**
851 **and impairs CDC20's interaction with its negative regulators MAD2 and PLK1.**

852 **(A)** Proximity ligation assay (PLA) of CLL-like MEC1 cells that were synchronized in
853 mitosis (9 μ M RO-3306 for 20h, 1h after release). TCL1A interacts with CDC20,
854 MAD2, and CDK1 during mitosis. Quantification of PLA foci per cell is displayed in
855 **Supplemental Figure 7A.** Images were taken using an SP8 confocal microscope
856 (Leica) **(B)** PLA for TCL1A and CDC20 was performed in MEC1 and HG3 CLL-like
857 cells (synchronized as in (A)) and PLA foci per cell were quantified in mitotic and
858 non-mitotic cells. Significantly more foci were counted in mitotic cells compared to
859 non-mitotic cells. Negative control for MEC1: no primary antibody staining (Backgr.).
860 Negative control for HG3: empty-vector transfected cells (TCL1A-negative HG3-EV)
861 stained with primary antibodies. Boxes display medians with 25th-75th percentiles and
862 whiskers min and max; N=25 cells (significances by one-way ANOVA). Representa-
863 tive immunofluorescent images are in **Supplemental Figure 7C.** **(C)** Split YFP-
864 reporter principle of the protein complementation assay (PCA). Signal emission in
865 living cells was induced upon non-covalent complementation of the N/C-terminal YFP
866 components if the TCL1A-bait and the 'candidate' protein interact for >0.5sec. As a
867 negative control, a construct encoding an ATG codon fused with the N-terminal part
868 of YFP (ATG-YFP) was used to exclude fluorescence derived from spontaneous
869 transient re-joining of split YFP parts. Images were taken on an Axio Scope.A1 mi-
870 croscope (Zeiss, Germany) at 100x magnification. **(D)** HeLa cells were co-
871 transfected with TCL1A-YFP^N and CDC20-YFP^C constructs and the TCL1A-CDC20
872 interaction was visualized by the YFP signal (green). Cytoskeleton and DNA were
873 visualized by rhodamine-phalloidin (red) and Hoechst (blue), respectively. Prominent
874 signals corresponding to the specific TCL1A-CDC20 interaction accumulated at the
875 mitotic plate and dispersed during anaphase. **(E)** Five constructs of indicated CDC20
876 variants were generated by PCR-mediated site-directed mutagenesis (top) and were
877 used in co-IPs in HEK293 cells to interrogate sequence restrictions of the CDC20-
878 TCL1A interaction (bottom). RCRY^{4A} and del(97-169) nearly completely abolished
879 the interaction. **(F)** The CDC20-TCL1A complex was predicted based on the pub-
880 lished experimental protein structures of CDC20 (pdb ID 4GGA) and TCL1A (pdb ID
881 1JSG). Predictive tools to propose putative interfaces (CPORT⁵⁹) were used and the
882 outputs exploited in the High Ambiguity Driven protein-protein DOCKing 2.2 (HAD-
883 DOCK 2.2) algorithm for modeling biomolecular complexes.⁴¹ This *in-silico* modeling
884 predicted 2 potential models, which differ in the amino acids (aa) of TCL1A involved
885 in this interaction. The residues E40, K42, Y96 of TCL1A are expected to stabilize
886 the TCL1A-CDC20 interaction in Model A, while E9, R93, Y96 would promote this

interaction in Model B. Detailed HADDOCK statistics are summarized in **Supplemental Tables 12 and 13.** **(G)** Top: TCL1A mutants used in co-IP studies. They represent Model A (EKY^{SAE} , in red) with the aa substitutions E40S, K42A, and Y96E, and Model B (ERY^{KDE} , blue) with E9K, R93D, and Y96E. Bottom: CDC20 co-IP of lysates from JVM3 cells stably overexpressing TCL1A-FLAG, TCL1A- EKY^{SAE} -FLAG, or TCL1A- ERY^{KDE} -FLAG. Cells were synchronized before in G2 by 9 μM RO-3306 for 20h. In the last five hours, 10 μM MG132 was added to reduce protein degradation of the two mutants. The EKY^{SAE} (Model A) nearly abolished the TCL1A-CDC20 interaction. **(H)** PLA for CDC20 and MAD2 was performed in MEC1-shTCL1A (TCL1A knock-down) vs. -shCtrl cells as well as in HG3-EV vs. -TCL1A (TCL1A introduction) cells. Significantly less PLA foci were counted per cell in the TCL1A-expressing / -high lines, suggesting an impaired CDC20-MAD2 interaction in the presence of TCL1A. Boxes display medians with 25th-75th percentiles and whiskers min and max; N=40 cells (significances as per Student's t-test). Images were taken using an SP8 confocal microscope (Leica). **(I)** JVM3 +/- TCL1A cells were synchronized in G2 by 9 μM RO-3306 for 20h and released in full medium. CDC20-IP was performed in lysates at indicated time points to determine CDC20-PLK1 interaction. IgG control: pooled lysates of JVM3^{EV} and JVM3^{TCL1A}.

905 **Figure 7. CDC20 expression is reduced in CLL and correlates with a more ag-**
 906 **gressive cell and disease phenotype.**

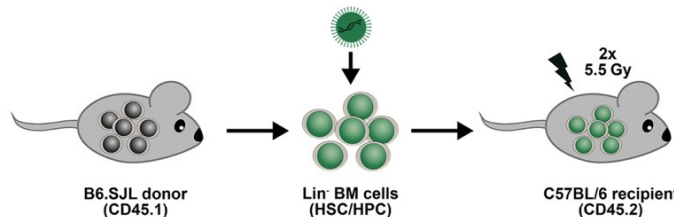
907 **(A)** *CDC20* expression in different lymphatic and myeloid neoplasms as measured by
 908 microarray-based gene expression profiling (dataset of Haferlach et al⁴⁹ on
 909 www.oncomine.org). Boxes with medians and 25th / 75th percentiles. Whiskers show
 910 10th and 90th percentiles. CLL stands out among the other hematopoietic cancers, as
 911 its *CDC20* expression is markedly reduced; e.g. FCh -6.8, $P<0.001$ compared to
 912 healthy controls (HC). **(B)** Expression of *TCL1A* and *CDC20* in primary human CLL
 913 cells. Left: representative immunoblot showing decreased *CDC20* expression in ly-
 914 sates from unstimulated IGHV unmutated U-CLL (N=6) vs M-CLL (N=6). Right: Line-
 915 ar regression analysis demonstrates an inverse correlation of *TCL1A* and *CDC20*
 916 protein levels in CLL (N=19, $P=0.002$; $R^2=0.437$). **(C)** Gene expression profiling
 917 (GEP) of N=337 previously untreated CLL patients of the prospective CLL8 trial iden-
 918 tified an inverse correlation of *TCL1A* (blue) and *CDC20* (green) expression. **(D)** Pa-
 919 tients from the CLL8 trial were divided into two groups by the median expression of
 920 *CDC20*. Patients with low *CDC20* expression (N=166, dark green) showed signifi-
 921 cantly higher white blood cell (WBC) counts in comparison to those with high *CDC20*
 922 (N=163, light green). Boxes show medians and the 25th/75th percentiles, whiskers the
 923 10th-90th percentiles. Significance was determined using the median-test. **(E)** Patients
 924 from the CLL8 trial that received fludarabine/cyclophosphamide (FC) were divided
 925 into two groups by the median expression of *CDC20*. The Kaplan-Meier curve illus-
 926 trates the significantly shorter progression-free survival (PFS) of patients with low
 927 *CDC20* expression (N=86, green, median PFS=25.5 months) compared to those with
 928 high *CDC20* expression (N=83, blue, median PFS=34.1 months), $P=0.014$, log-rank
 929 test. **(F)** *CDC20* expression levels are significantly lower in CLL than in those
 930 characterized by a molecular profile of genome instability (N=189)²⁹ than in those
 931 with activation of epithelial-mesenchymal-transition (EMT)-like programs (N=130;
 932 $P<0.001$, Mann-Whitney test). Boxes with medians, 25th/75th percentiles, and whisk-
 933 ers of min./max. **(G)** Reanalysis of single-cell RNA-sequencing data from *Eμ-TCL1A*
 934 and *Eμ-TCL1A^{Akt-C}* (Richter's syndrome model) mice that we published in Kohlhaas et
 935 al³⁰. The UMAP displays the clusters identified in the integrative analysis of both
 936 models that were then applied to the *Eμ-TCL1A* model only (N=4 mice). Clusters 2
 937 and 10 are enriched in *Eμ-TCL1A* cells, while clusters 0, 3, 13, 18, 19, and 20 repre-
 938 sent *Eμ-TCL1A^{Akt-C}* or those that are shared with *Eμ-TCL1A*. **(H)** *Cdc20* is primarily
 939 expressed in the *Eμ-TCL1A* enriched Seurat cluster 2. **(I)** *TCL1A* expression is signif-
 940 icantly lower in Seurat cluster 2 compared to all other clusters, $P<0.001$, **Supple-**
941 mental Table 16. **(J)** Setup of *in vivo* *Cdc20* knock-down experiment: leukemic *Eμ-*

942 *TCL1A* splenocytes⁵⁰ were nucleofected with the transposon-based pJ547-shCdc20
943 construct. It encodes a GFP cassette with miR-30-based shRNA sequences against
944 murine Cdc20 at the 3'-end. A pJ547-GFP control encoded an unspecific shRNA
945 sequence. After i.p. injection into syngeneic hosts and tumor development, GFP+
946 splenocytes were FACS-purified and re-injected into hosts. Knock-down efficiency
947 was tested by immunoblots (right). **(K)** Flow-cytometric analysis of peripheral-blood
948 cells showing a faster increase of the aberrant leukemic Cd5+ Cd19+ B-cell popula-
949 tion in recipients that were transplanted with *Eμ-TCL1A;Cdc20-KD* B-cells (N=19)
950 compared to *Eμ-TCL1A;GFP* control animals (N=15). Boxes indicate medians and
951 25th/75th percentiles and whiskers show min. / max.; significance was tested using a
952 two-way ANOVA with Bonferroni correction for multiple testing. **(L)** Immunoblot anal-
953 ysis showing increased Cyclin D1 and slightly reduced PARP cleavage in spleno-
954 cytes from *Eμ-TCL1A;Cdc20-KD* compared to *Eμ-TCL1A;GFP* mice. Splenocytes
955 were isolated at the endpoint of survival analysis. Each lane represents an individual
956 animal. **(M)** The proportion of metaphases with an aberrant number of chromosomes
957 was significantly higher in *Eμ-TCL1A;Cdc20-KD* cells compared to *Eμ-TCL1A;GFP*
958 cells (Student's t-test).

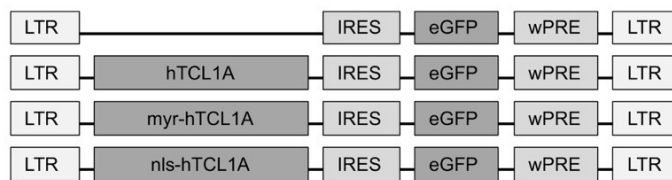
Figure 1

A

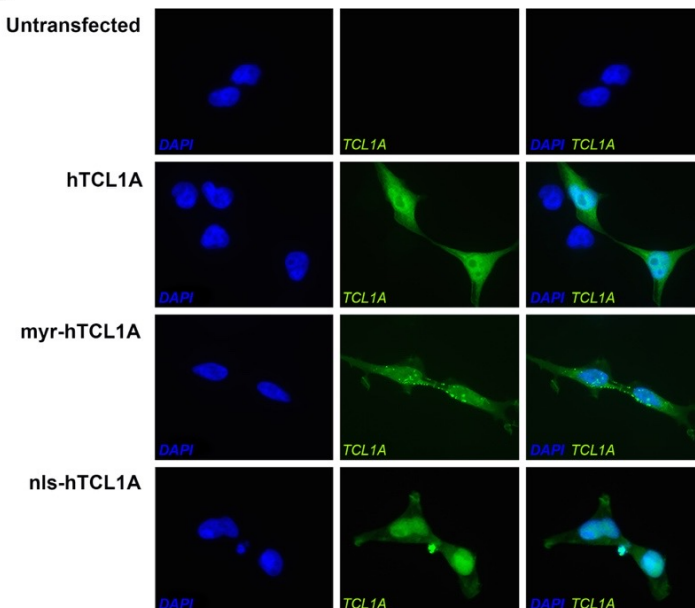
Adoptive transfer model of TCL1A transgenic stem cells



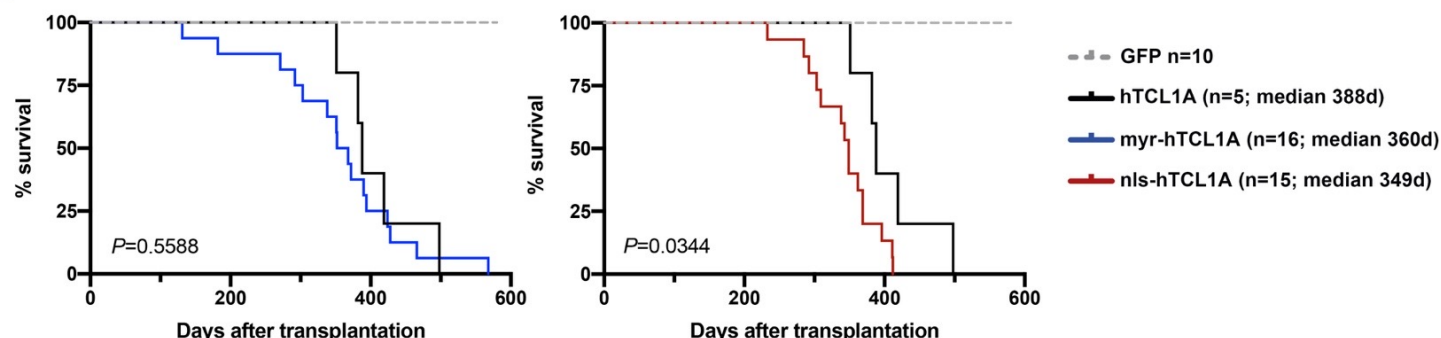
Vectors for the 4 mouse cohorts:



B

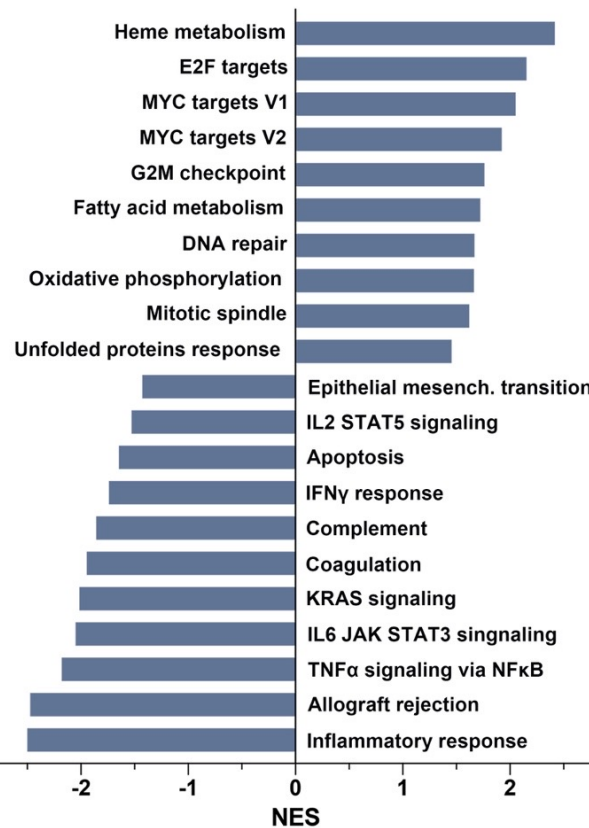


C



D

GSEA nls-hTCL1A vs hTCL1A



E

Enrichment plots nls-hTCL1A vs hTCL1A

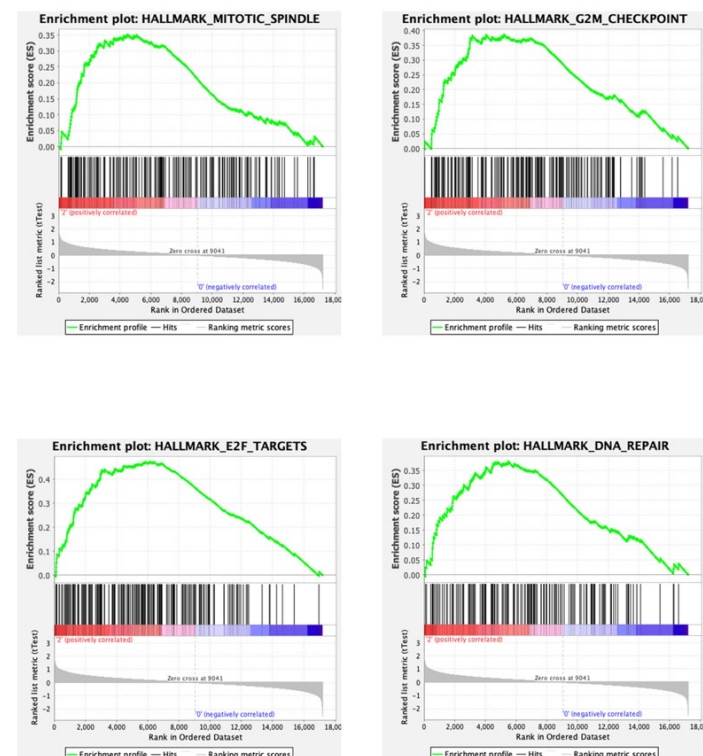


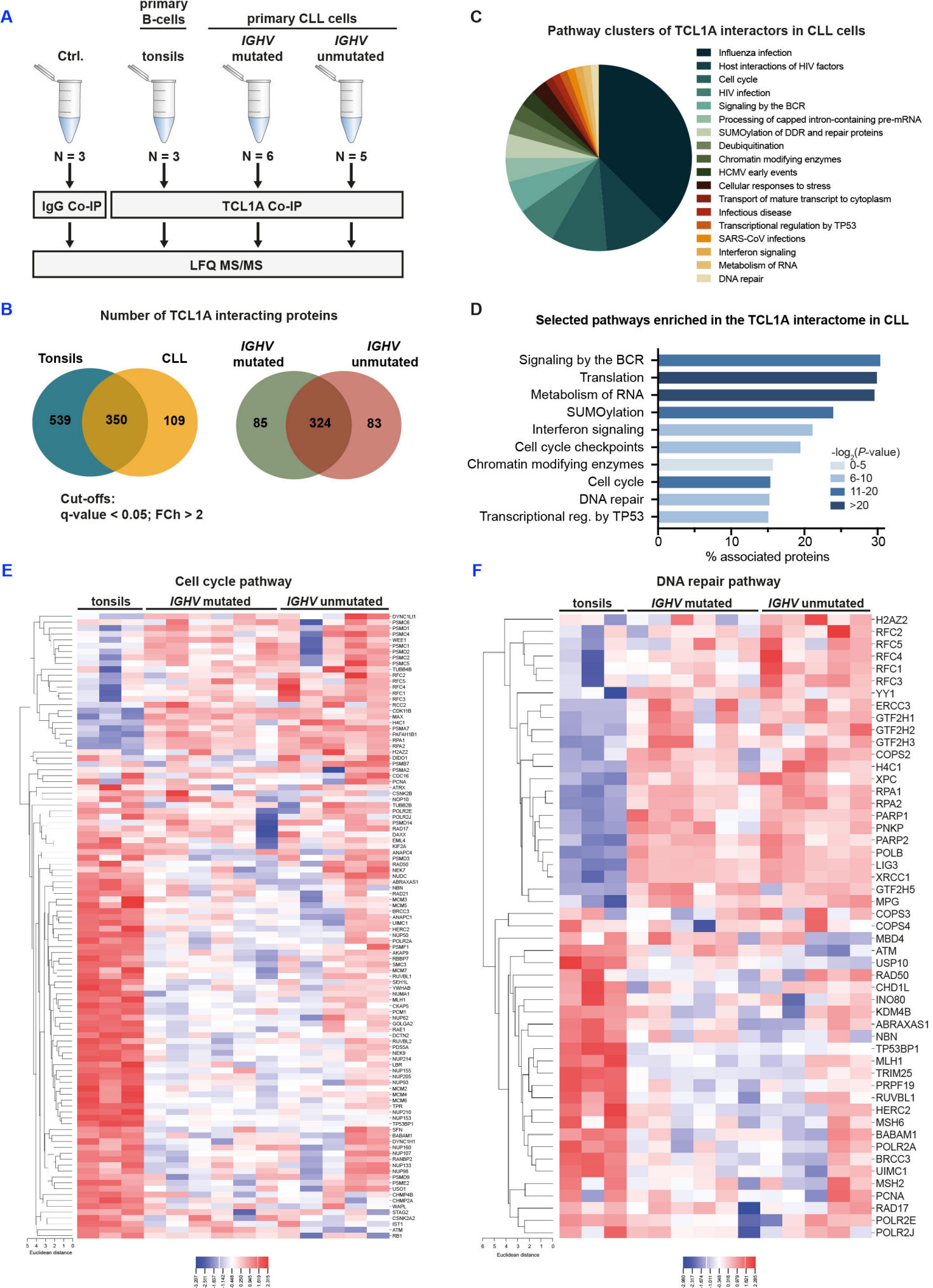
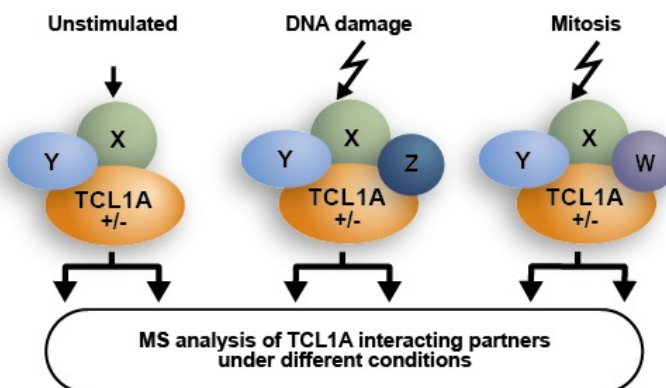
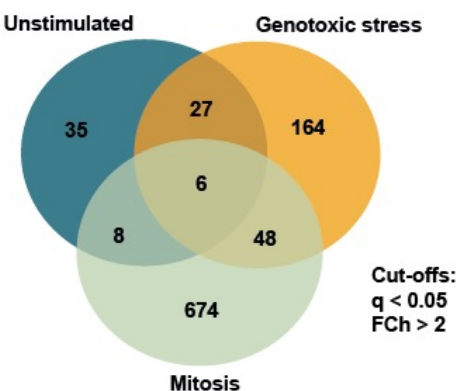
Figure 2

Figure 3

A



B



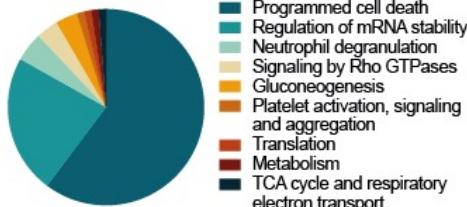
C

Pathway clusters of TCL1A interactors identified by ClueGo

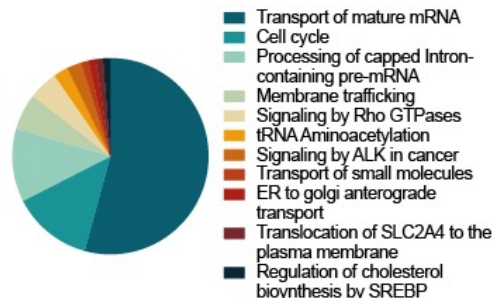
Unstimulated cells, N unique proteins = 35:



Genotoxic stress, N unique proteins = 164:

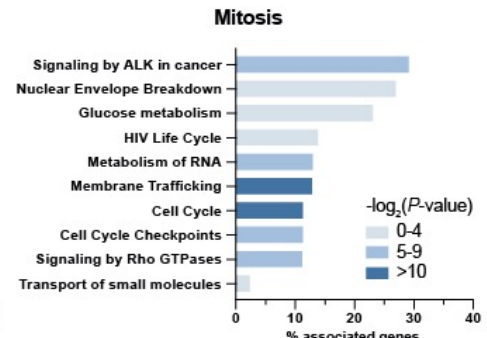
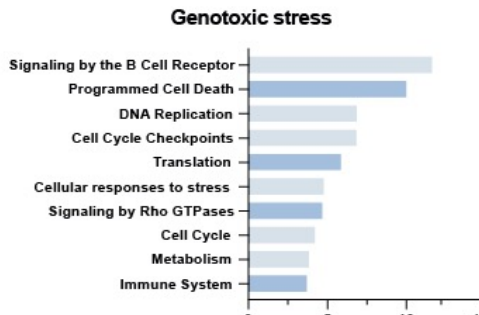
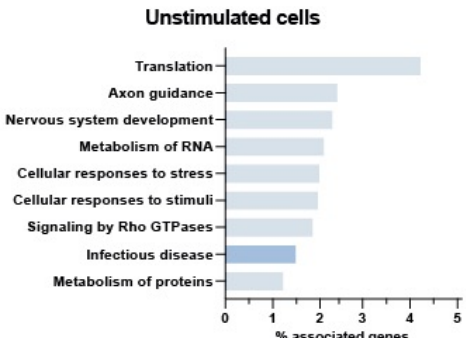


Mitosis, N unique proteins = 674:



D

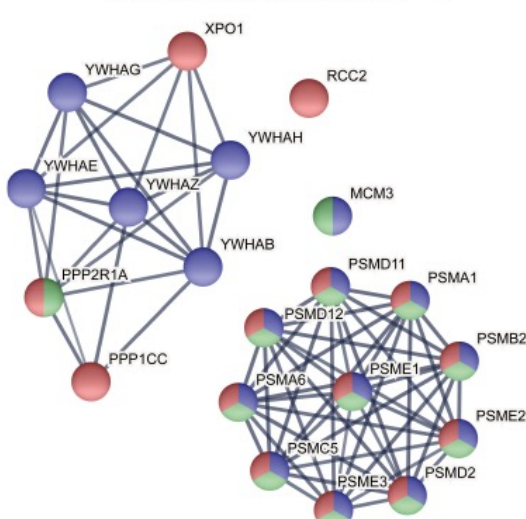
Selected Reactome pathways enriched in the interactome of TCL1A



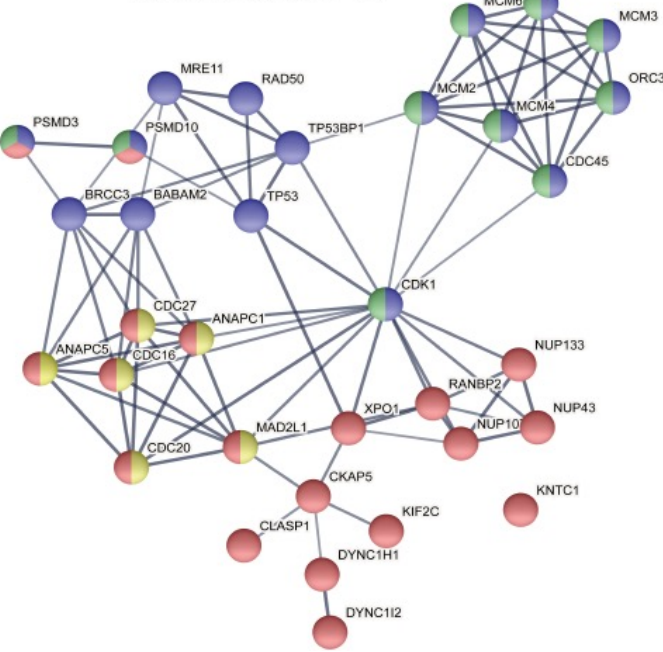
E

STRING network of proteins involved in the Cell Cycle Checkpoint Pathway

Condition: Genotoxic stress, N = 20



Condition: Mitosis, N = 33



Involved in pathway:

G1/S Transition, G2/M Checkpoint, Separation of Sister Chromatids, Inhibition of APC/C via Direct Inhibition of the APC/C Complex

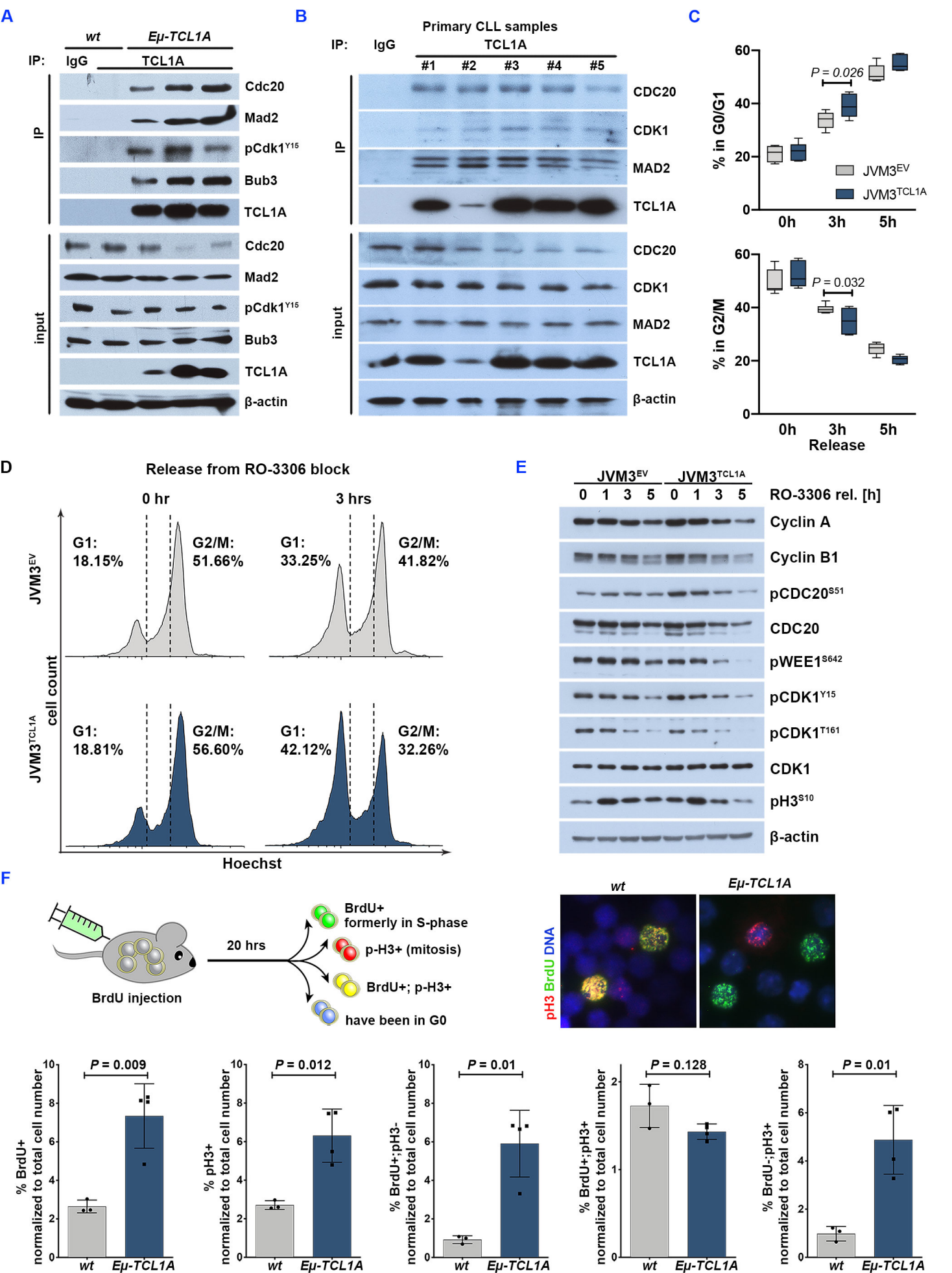
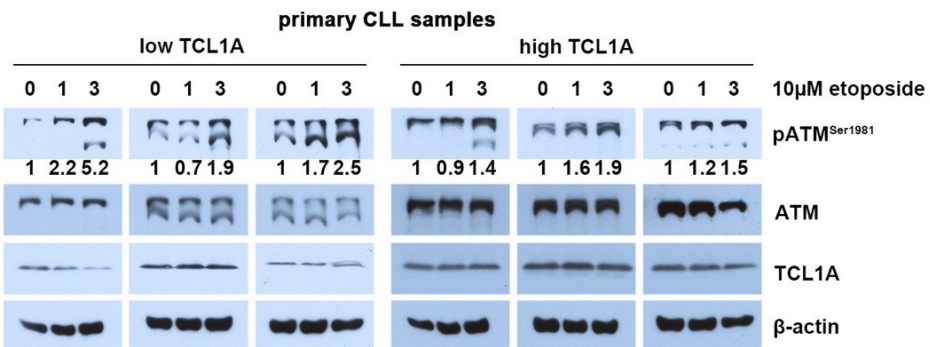
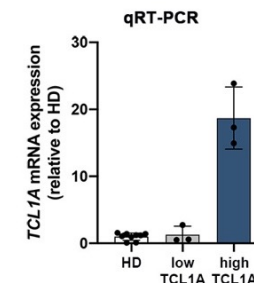
Figure 4

Figure 5

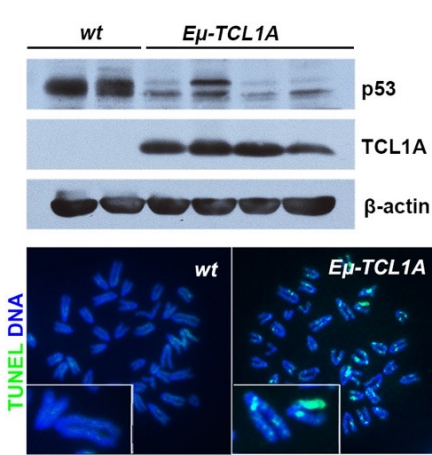
A



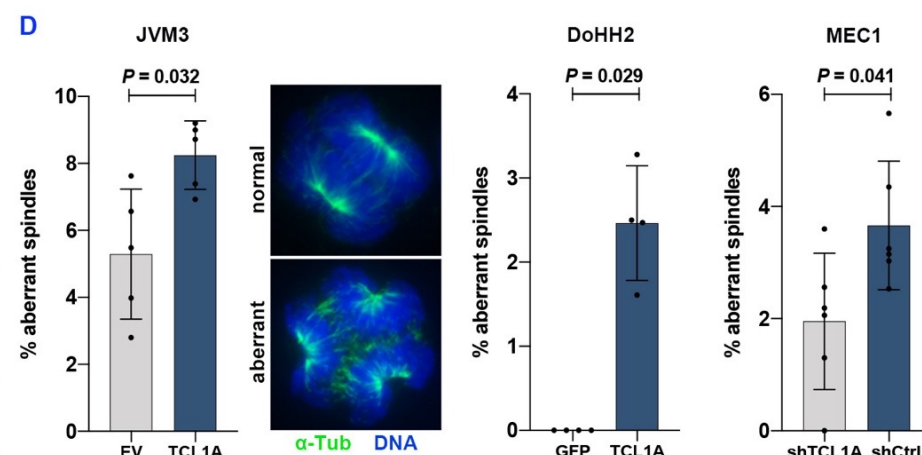
B



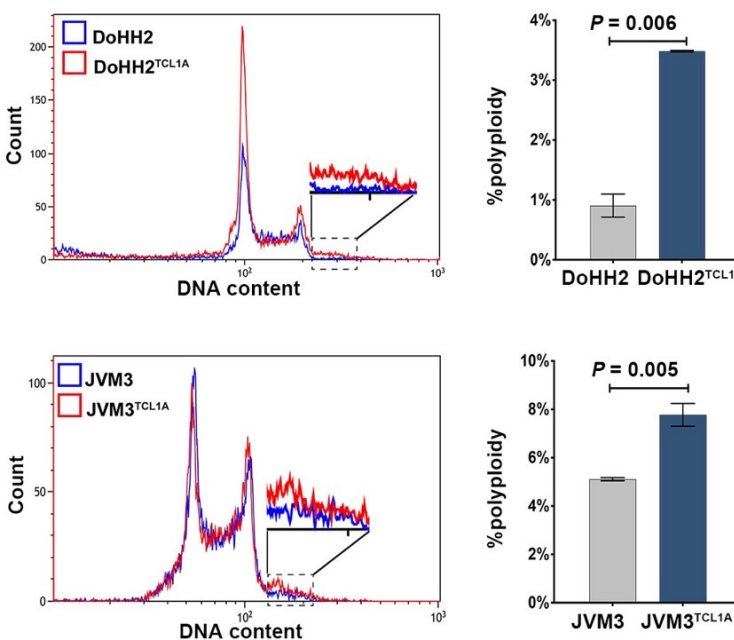
C



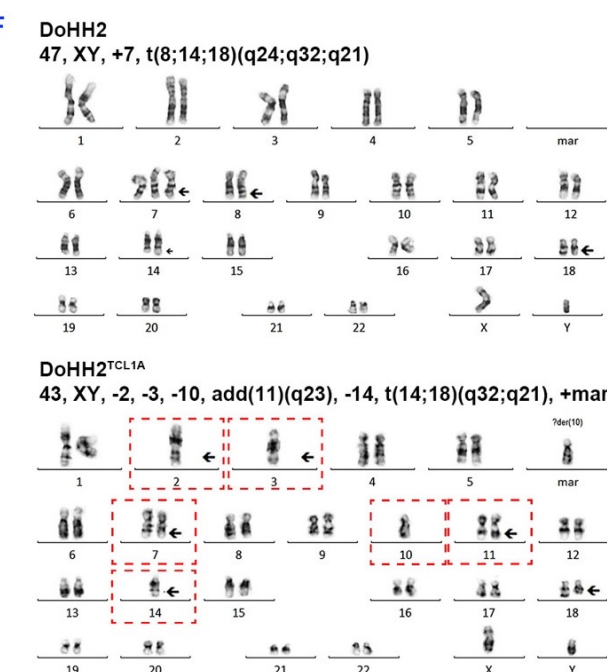
D



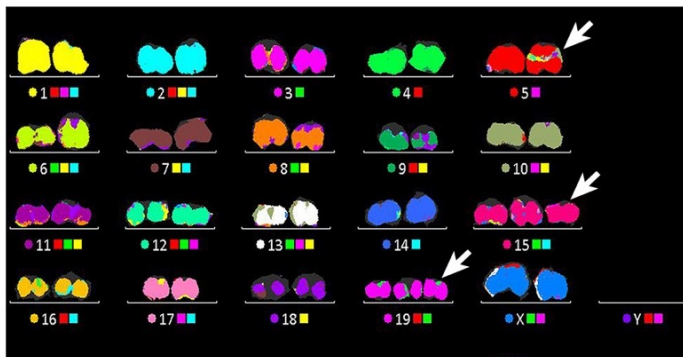
E



F



G



H

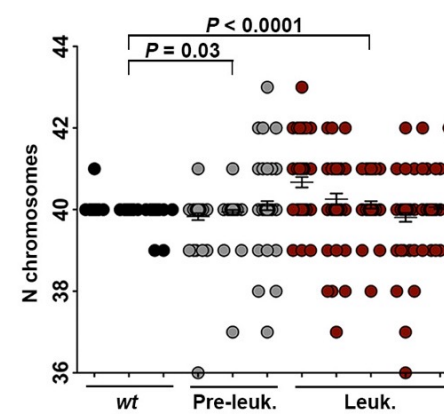


Figure 6

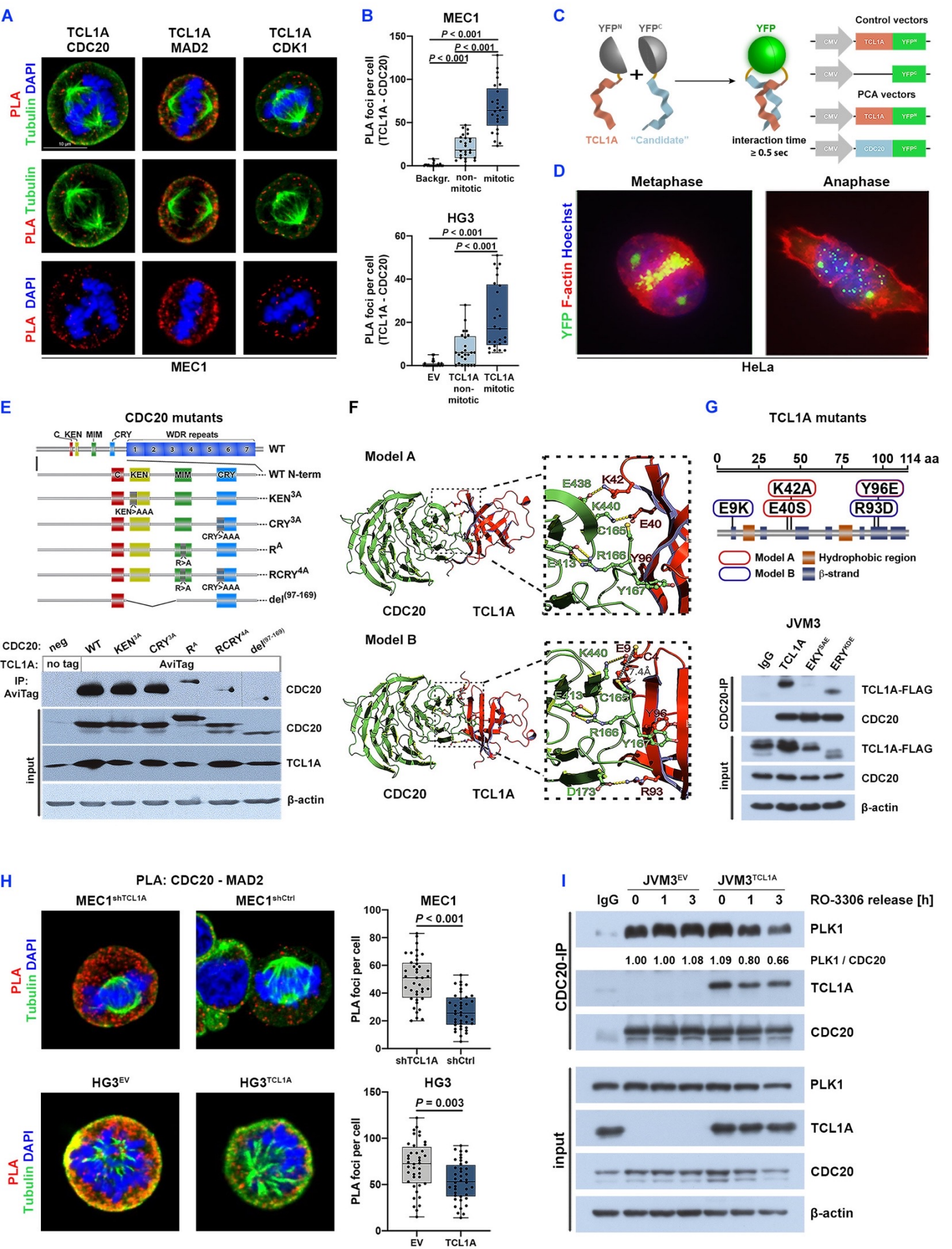


Figure 7

